Afterslip and aftershocks in the rate-and-state friction law

Agnès Helmstetter[1] and Bruce E. Shaw[2]

[1]   We study how a stress perturbation generated by a main shock affects a fault obeying the rate-state friction law using a simple slider block system. Depending on the model parameters and on the initial stress, the fault exhibits aftershocks, slow earthquakes, or decaying afterslip. We found several regimes with slip rate decaying as a power law of time, with different characteristic times and exponents. The behavior of the rate-state friction law is thus far more complex than described by the "steady state" approximation frequently used to fit afterslip data. The fault reaches steady state only at very large times, when slip rate has decreased to the tectonic loading rate. The complexity of the model makes it unrealistic to invert for the friction law parameters from afterslip data. We modeled afterslip measurements for three earthquakes using the complete rate-and-state law and found a huge variety of model parameters that can fit the data. In particular, it is impossible to distinguish the stable velocity-strengthening regime ($A > B$) from the (potentially) unstable velocity-weakening regime ($A < B$). Therefore, it is not necessary to involve small-scale spatial or temporal fluctuations of friction parameters A or B in order to explain the transition between stable sliding and seismic slip. In addition to B/A and stiffness, the fault behavior is strongly controlled by stress levels following an event. Stress heterogeneity can thus explain part of the variety of postseismic behaviors observed in nature. Afterslip induces a progressive reloading of faults that are not slipping, which can trigger aftershocks. Using the relation between stress and seismicity derived from the rate-and-state friction law, we estimate the aftershock rate triggered by coseismic and postseismic slip. Aftershock rate does not simply scale with stress rate but exhibits different characteristic times and sometimes a different power law exponent. Afterslip is thus a possible candidate to explain observations of aftershock rate decaying as a power law of time with an Omori exponent that can be either smaller or larger than 1. Progressive unloading due to afterslip can also produce delayed seismic quiescence.

1.   Introduction

[2]   Most shallow large earthquakes are followed by significant postseismic deformation, and by an increase in seismic activity, which can last for several years. The link between aseismic afterslip and aftershock activity is however not clear. The cumulative moment released by aftershocks is usually much lower than the one associated with afterslip, which implies that postseismic deformation is unlikely to be due to aftershock activity. The similar time decay and duration of postseismic deformation and aftershocks rather suggests that aftershocks are induced by afterslip [*Wennerberg and Sharp*, 1997; *Schaff et al.*, 1998; *Perfettini and Avouac*, 2004, 2007; *Perfettini et al.*, 2005; *Hsu et al.*,

2006; *Savage et al.*, 2007]. But there are alternative models which explain aftershock triggering by the static [*Dieterich*, 1994] or dynamic [*Gomberg et al.*, 1998] stress change associated with the main shock, or by fluid flow [*Nur and Booker*, 1972].

[3]   Postseismic deformation is most often localized around the rupture zone, and is thus modeled as afterslip on the main shock fault. However, there are observations of long-range diffuse deformation following large earthquakes [*Nur and Mavko*, 1974], which can be modeled by viscoelastic relaxation of the lower crust or upper mantle. Another potential candidate for postseismic deformation is poroelastic deformation. At large depth below the seismogenic zone, a ductile creep law may be more appropriate than friction laws [*Montési*, 2004]. Distinguishing between the different mechanisms is difficult on the basis of available data [*Montési*, 2004]. In some cases, several processes have to be involved to fit the data [*Deng et al.*, 1998; *Pollitz et al.*, 2006; *Freed et al.*, 2006a]. Afterslip is often comparable with coseismic slip (see *Pritchard and Simons* [2006] for a review on afterslip in subduction zones), even if there are very large

[1]Laboratoire de Géophysique Interne et Tectonophysique, Université Joseph Fourier and Centre National de la Recherche Scientifique, Grenoble, France.
[2]Lamont-Doherty Earth Observatory, Columbia University, Palisades, New York, USA.

variations in the amount of afterslip from one event to another one [*Melbourne et al.*, 2002; *Marone*, 1998; *Pritchard and Simons*, 2006]. For instance, the *M*7.6 1994 Sanriku-Haruka-Oki earthquake in Japan had very large afterslip, with cumulative seismic moment a little larger than the coseismic moment [*Heki et al.*, 1997]. *Takai et al.* [1999] also reported afterslip as large, in term of seismic moment, as coseismic slip for a much smaller *M* = 5.7 earthquake in the same area. For the 2004 Parkfield event, the moment of the postseismic slip for the first 60 days was about twice the coseismic moment [*Langbein et al.*, 2006].

[4] The rate-and-state friction law, introduced by *Dieterich* [1979] based on laboratory friction experiments, has been frequently used to model both afterslip [e.g., *Marone et al.*, 1991], slow earthquakes [e.g., *Yoshida and Kato*, 2003; *Liu and Rice*, 2005], and seismic activity [e.g., *Dieterich*, 1994]. Depending on the parameters of the rate-and-state friction law, the model is either stable (aseismic slip), or able to produce slip instabilities (earthquakes). In the unstable regime, the rate-and-state friction law provides a relation between stress history and seismicity [*Dieterich*, 1994]. This relation can be used to predict the seismicity rate triggered by any stress change, such as static [*Dieterich*, 1994] or dynamic [*Gomberg et al.*, 1998] stress change induced by a main shock, postseismic slip, or transient deformation associated with intrusions or eruptions [*Dieterich et al.*, 2000], slow earthquakes [*Segall et al.*, 2006; *Lohman and McGuire*, 2007] or tides [*Cochran et al.*, 2004]. Extensions of the original theory to include stress heterogeneity as a fundamental aspect of aftershock process has further improved matches with observations, including where aftershocks occur and modifications to the time dependence of the decay [*Marsan*, 2006; *Helmstetter and Shaw*, 2006]. This extension explains why many aftershocks occur on the main shock rupture area, where stress decreases on average after the main shock, but with stress heterogeneity both stress increases and stress decreases occur.

[5] Previous studies have modeled afterslip using the rate-and-state friction law [*Rice and Gu*, 1983; *Scholz*, 1990; *Marone et al.*, 1991; *Boatwright and Cocco*, 1996; *Marone*, 1998; *Wennerberg and Sharp*, 1997; *Schaff et al.*, 1998; *Hearn et al.*, 2002; *Hearn*, 2003; *Miyazaki et al.*, 2004; *Johnson et al.*, 2006], or a simpler rate-dependent friction law [*Montési*, 2004; *Perfettini and Avouac*, 2004, 2007; *Perfettini et al.*, 2005; *Langbein et al.*, 2006; *Hsu et al.*, 2006]. Most of these studies have assumed that afterslip is associated with stable faults in the velocity-strengthening regime. They have also assumed that faults are close to the steady state regime during afterslip. With this approximation, the friction coefficient only depends on slip velocity, which simplifies the analysis. Most of these studies used slider block models, with one or a few blocks, but recent studies have developed continuous faults models [*Hearn et al.*, 2002; *Hearn*, 2003; *Johnson et al.*, 2006; *Perfettini and Avouac*, 2007], which can account for heterogeneity of slip and of friction law parameters, and elastic interactions between different parts of the faults. All models have been rather successful in matching afterslip data. However, they also bring new problems.

[6] While most afterslip usually occur above [*Marone et al.*, 1991; *Marone*, 1998; *Hsu et al.*, 2006] or below [*Langbein et al.*, 2006; *Perfettini and Avouac*, 2007] the seismogenic zone, in many cases some afterslip is also found at the same depth as coseismic slip [*Hearn et al.*, 2002; *Miyazaki et al.*, 2004; *Langbein et al.*, 2006; *Johnson et al.*, 2006; *Hsu et al.*, 2006]. Aftershock zones also frequently overlap with afterslip areas [*Miyazaki et al.*, 2004; *Langbein et al.*, 2006; *Hsu et al.*, 2006, 2007; *Perfettini and Avouac*, 2007]. In the case of 1999 Izmit earthquake, there was a large patch of aseismic slip around the hypocenter [*Bürgmann et al.*, 2002], in contradiction with the common assumption that afterslip is limited to velocity-strengthening zones. To account for these observations, some researchers invoked either small-scale spatial [*Miyazaki et al.*, 2004; *Johnson et al.*, 2006] or temporal [*Wennerberg and Sharp*, 1997; *Hearn et al.*, 2002] variations in the friction parameters. The mixing of small-scale spatial variations of stably sliding and unstably sliding is the most widely proposed explanation. Only *Boatwright and Cocco* [1996] evoked the possibility that afterslip can be produced by faults that are slightly velocity weakening. They used numerical simulations of a spring slider system to model crustal faulting, including dynamic rupture, aftershock triggering and aseismic slip events. *Boettcher and Jordan* [2004] also suggested that, for mid-ocean ridge transform faults, seismic and subseismic slip can occur on the same fault patch.

[7] In this work, we study analytically and numerically the postseismic slip in the rate-and-state model, without using the steady state approximation. We show that afterslip and slow earthquakes are not limited to stable faults, but can also occur in seismogenic zones. We also fit the model to the afterslip data measured following the 2000 M_w8 Denali earthquake [*Freed et al.*, 2006a, 2006b], the 2004 M_w6 Parkfield earthquake [*Langbein et al.*, 2006], and the 2005 $M_w8.7$ Nias event [*Hsu et al.*, 2006].

[8] Afterslip transfers stress from sliding to locked parts of the fault, and is thus a potential mechanism for aftershock triggering [*Boatwright and Cocco*, 1996; *Wennerberg and Sharp*, 1997; *Schaff et al.*, 1998; *Perfettini and Avouac*, 2004; *Hsu et al.*, 2006; *Bourouis and Bernard*, 2007]. *Dieterich* [1994] demonstrated that postseismic stressing following an earthquake can reproduce an Omori law decay of aftershocks. The suggestion that afterslip triggers aftershocks is based on the observation that both afterslip and aftershock rate roughly decay as the inverse of the time since the main shock. There is as well some spatial correlation between the inferred location of afterslip and aftershocks [*Hsu et al.*, 2006]. However, there is a priori no reason to expect that aftershock rate is proportional to stress rate. In particular, in the rate-and-state friction model, earthquakes can be triggered at very long times following a stress change. The relation between stress history and seismicity rate is indeed complex and nonlinear [*Dieterich*, 1994]. We thus use the complete rate-and-state friction law in order to model afterslip and aftershock activity.

2. Modeling Aftershocks, Afterslip, and Slow Earthquakes With the Rate-and-State Friction Law

2.1. Slider Block Model With Rate-and-State Friction

[9] We use the rate-and-state friction formulation of *Ruina* [1983], based on *Dieterich* [1979]

$$\mu = \mu^* + A \ln \frac{V}{V^*} + B \ln \frac{\theta V^*}{D_c}. \tag{1}$$

Table 1. Notations

Parameter	Equation	Description
A, B	(1)	coefficient of the rate-and-state direct and evolution effects
c		characteristic time of Omori law for aftershock rate
δ	(4)	slip
D_c	(2, 3)	characteristic slip distance
G	(5)	shear modulus
γ	(52)	seismicity state variable, inversely proportional to seismicity rate
k k_c, k_B	(4, 7, 13)	spring stiffness, and threshold for slip instabilities and accelerations
μ, μ^*, μ_0	(1, 4)	friction coefficient, characteristic and initial value
$\mu_{ss}(V)$	(6)	friction coefficient at steady state
$\mu_a(V)$, $\mu_l(V)$	(15, 8)	friction threshold for slip accelerations and instabilities
l, l_c	(5)	crack length and critical value
m	(60)	ratio of characteristic stress change and $A\sigma$
N	(55)	cumulative number of aftershocks
θ, θ_0	(2, 3)	state variable and initial value
p	(48)	exponent of slip rate decay
ρ		Omori exponent for aftershock rate
$R(t)$, R_0	(51)	seismicity rate, and initial value just after stress change
r	(52)	seismicity rate at constant stressing rate equal to $\dot{\tau}_l$
σ	(4)	normal stress
t		time since main shock
t_0, t_1, t^*	(19, 27, 45, 48)	characteristic times for afterslip (start of power law decay)
t_a	(28)	duration of the nucleation phase-characteristic time of tectonic loading
t_i	(34, 35)	time of slip instability
t_c	(64)	crossover time for aftershock rate
t_m	(61)	time of seismicity rate peak
τ, τ_0, τ_l	(4)	shear stress, initial value and tectonic load
$\tau_{\max}$	(63)	maximum stress change due to afterslip
$\Delta\tau$	(51)	coseismic stress change
V, V^*, V_0,	(1, 9)	slip rate, characteristic and initial values
V_l, V_1, V_2	(23, 50)	constant loading rate

where μ^* and V^* are constants, A and B are friction parameters, D_c is the critical slip distance, and θ is the state variable, which will evolve with slip and time. The state variable is often interpreted as the average age of contacts on the fault. All notations are listed in Table 1.

[10] Most experimentally derived values of D_c are of order 1 to 100 μm [*Marone*, 1998]. There is much debate whether these values are applicable to real faults. The critical slip distance is found experimentally to increase with fault roughness and with the gouge layer thicknesses [*Marone*, 1998], so it may be larger for real faults. Large values of the slip weakening distance, of the order of 0.1 to 1 m, are usually inferred from seismic inversions [e.g., *Ide and Takeo*, 1997], or from friction experiments at high slip rate due to frictional heating [*Tsutsumi and Shimamoto*, 1997] or melting [*Hirose and Shimamoto*, 2005], or to the formation of a thin layer of silica gel on the fault surface [*Goldsby and Tullis*, 2002; *Di Toro et al.*, 2004]. Seismological inferences are, however, generally only upper bounds, owing to bandwidth limitations [*Guatteri and Spudich*, 2000].

[11] The friction parameters A and B are of the order of 0.01 and are found experimentally to depend on environmental conditions such as temperature and on the fault gouge properties [*Scholz*, 1990; *Marone*, 1998]. For real faults, a first transition is expected from velocity strengthening to velocity weakening associated with the transition from unconsolidated gouge to lithified and indurated gouge. A second transition between velocity weakening and velocity strengthening is expected at a temperature of about 300°C. This model thus explains the distribution of seismicity with depth [*Scholz*, 1990].

[12] There are a couple of evolution laws for the state variable that have been proposed by *Ruina* [1983] to explain the friction experiments of *Dieterich* [1979]. Most studies who used the rate-and-state friction to model aftershocks, afterslip or slow earthquakes used the aging law [*Marone et al.*, 1991; *Dieterich*, 1994; *Liu and Rice*, 2005, 2007]

$$\frac{d\theta}{dt} = 1 - \frac{V\theta}{D_c}. \tag{2}$$

In the slip law, the state variable obeys

$$\frac{d\theta}{dt} = -\frac{V\theta}{D_c} \ln \frac{V\theta}{D_c}, \tag{3}$$

Recent experimental works suggest that this law may better explain experimental data for large changes in slip rate [*Bayart et al.*, 2006], but it does not explain changes in friction with time at zero slip velocity [*Beeler et al.*, 1994]. The slip law may be more adapted to study the nucleation phase, while the aging law may be better for the interseismic phase [*Ampuero and Rubin*, 2008]. In this work, we chose the aging law for its simplicity and to compare with previous studies on afterslip. We also performed numerical simulations with the slip law. We found that both evolution laws produce qualitatively similar behaviors (afterslip, slow earthquakes, and aftershocks), but that the slip law is more unstable than the aging law. For instance, the range of parameters that produce slow earthquakes is smaller for the slip law than for the aging law.

[13] Following *Rice and Gu* [1983], *Gu et al.* [1984], and *Dieterich* [1992], we model a fault by a slider spring system. The slider represents either a fault or a part of the

fault that is sliding. The stiffness k represents elastic interactions between the fault patch and the ductile deeper part of the fault, that is assumed to creep at a constant rate. This simple model assumes that slip, stress and friction law parameters are uniform on the fault patch. The friction coefficient of the block is given by

$$\mu = \frac{\tau}{\sigma} = \frac{\tau_l - k\delta}{\sigma}, \qquad (4)$$

where k is the spring stiffness, σ is the normal stress, τ the shear stress on the interface, τ_l is the remotely applied stress acting on the fault in the absence of slip, and $-k\delta$ is the decrease in stress due to fault slip. We consider the case of a constant stressing rate $\dot{\tau}_l = kV_l$, where V_l is the load point velocity. The initial stress may be smaller or larger than steady state friction owing to coseismic slip on the fault patch or on adjacent parts of the fault. Expression (4) neglects inertia, and is thus only valid for low slip speed in the interseismic period. The stiffness is a function of the crack length l and shear modulus G [*Dieterich*, 1992]

$$k \approx G/l. \qquad (5)$$

In the steady state regime $\dot{\theta} = 0$, the friction law (1) becomes

$$\mu_{ss}(V) = \mu* + (A - B) \ln \frac{V}{V*}, \qquad (6)$$

both for the aging and slip laws. If $A < B$, friction at steady state decreases with slip rate ("velocity-weakening" regime). In the case $A > B$, $\mu_{ss}(V)$ increases with V ("velocity-strengthening" regime). The ratio B/A is thus the main parameter that controls the behavior of the model.

[14] Depending on the parameters B/A, k/k_c, and on the initial stress, the system exhibits either afterslip, slow earthquakes, or a slip singularity (aftershock). We define "afterslip" as aseismic slip at continuously decreasing slip rate. The term "slow earthquakes" is used to describe cases when slip rate accelerates but then decreases without producing a slip instability. We call an "aftershock" a fault that accelerates up to instability. In the absence of tectonic loading, slow earthquakes occur only if the fault if loaded above steady state by the main shock. If a tectonic loading is introduced, slow earthquakes can be produced even if initial stress is below steady state.

2.2. Stability Condition

[15] A linear stability analysis of the steady state of the rate-and-state friction law with both evolutions laws was done by *Ruina* [1983]. A nonlinear stability analysis was later performed by *Gu et al.* [1984] for the slip evolution law and by *Ranjith and Rice* [1999] for the aging law. Stability is controlled by the ratio B/A, by the initial friction μ_0 and slip rate V_0, and by the ratio k/k_c, where the critical stiffness is defined by *Ruina* [1983]

$$k_c = \frac{\sigma(B - A)}{D_c}. \qquad (7)$$

Note that k_c defined by (7) is negative for $A > B$. For a fault patch of length l in an elastic medium, the condition $k < k_c$ is equivalent to $l > l_c \approx G/k_c$ [*Dieterich*, 1992].

[16] For a one degree of freedom slider block driven at constant loading velocity V_l with the aging law (2), the

conditions of stability are [*Ranjith and Rice*, 1999] (1) for $A > B$ the fault evolves toward the steady state regime $V = V_l$, and slip instabilities never occur, as for the slip law; (2) for $A < B$ and with a constant loading rate V_l, the system is unstable for $k < k_c$ (V goes to infinity in finite time) and stable for $k > k_c$ (V evolves toward V_l at large times); (3) for $A < B$, $k < k_c$ and $V_l = 0$, the system is unstable if initial stress is larger than $\mu_l(V)$ defined by

$$\mu_l(V) = \mu_{ss}(V) - B \ln(1 - k/k_c), \qquad (8)$$

and stable for $\mu < \mu_l(V)$.

[17] The slip law is more unstable than the aging law. Slip singularities can occur in the slip law even when $k > k_c$ for large stress steps [*Gu et al.*, 1984], but do not exist for the aging law in this case. In the slip law, the stress at the stability boundary is $\mu_{ss}(V) + Bk/k_c$ [*Gu et al.*, 1984], smaller than in the aging law (8).

2.3. Condition for Initial Acceleration

[18] In addition to the stability of the model, which provide the asymptotic slip rate at large time, we are also interested in the short-time behavior. Even in the unstable regime, the slip instability can be preceded by a transient decrease in slip rate (afterslip). Stable systems can produce transient accelerations of slip rate which do not reach instability, i.e., slow earthquakes. In order to obtain slip accelerations, we need both small enough stiffness and large enough stress. For large stiffness, slip of the block induces a large decrease of stress, that results in decelerating slip rate. The maximum stiffness able to produce slip accelerations has been derived previously [*Dieterich*, 1992; *Rubin and Ampuero*, 2005; *Perfettini and Ampuero*, 2008]. We estimate below the friction threshold above which slip accelerates. We first consider the case where the loading rate is negligible, because we are primarily interested in modeling afterslip and slow earthquakes triggered by a stress perturbation.

[19] We rewrite the rate-and-state friction law (1) and (4) as

$$V = V_0 \, e^{\frac{\tau_l - k\delta}{A\sigma}} \left(\frac{\theta}{\theta_0} \right)^{-B/A}, \qquad (9)$$

where V_0 and θ_0 are the initial values of V and θ respectively. Taking the time derivative of (9), acceleration of the slider is given by

$$\dot{V} = V \left(\frac{\dot{\tau}_l - kV}{A\sigma} - \frac{B\dot{\theta}}{A\theta} \right). \qquad (10)$$

Thus slip accelerates if

$$\frac{\dot{\theta}}{\theta} < \frac{\dot{\tau}_l - kV}{\sigma B}. \qquad (11)$$

If slip rate is much larger than the loading rate, we can drop out the term $\dot{\tau}_l$ in (10). Using the state evolution law (2), we get the limit value for the state rate

$$\dot{\theta}_a = \frac{1}{1 - B\sigma/kD_c} = \frac{1}{1 - k_B/k}, \qquad (12)$$

where the characteristic stiffness k_B is defined by

$$k_B = \frac{B\sigma}{D_c}. \qquad (13)$$

By definition of the state variable (2), state rate is always less than 1. This implies that accelerations are possible only for $\dot{\theta}_a < 1$, which is equivalent to $k < k_B$ [*Dieterich*, 1992; *Perfettini and Ampuero*, 2008].

[20] We can rewrite equations (1, 2, and 6) to get a relation between friction and state rate

$$\mu = \mu_{ss}(V) + B\ln(1 - \dot{\theta}), \qquad (14)$$

which gives the value of the friction $\mu_a(V)$ corresponding to $\dot{V} = 0$

$$\mu_a(V) = \mu_{ss}(V) - B\ln(1 - k/k_B). \qquad (15)$$

For $k < k_B$, the minimum stress necessary to produce an acceleration $\mu_a(V)$ is thus larger than its steady state value. As stiffness k/k_B decreases, this threshold decreases toward $\mu_{ss}(V)$. It is thus much easier to produce slip accelerations.

[21] Slip accelerations can occur as well for velocity-weakening or velocity-strengthening faults, as noted previously [*Dieterich*, 1992], because parameter A does not appear in equations (13) and (15). However, if $A > B$, "the displacement during unstable slip may be quite small, because θ will soon evolve to steady state, velocity strengthening, which will stabilize the slip" [*Dieterich*, 1992].

[22] We found in numerical simulations that the stability of the system is controlled both by the initial sign of $\dot{V}$ and $\dot{\theta}$. If both V and $\dot{\theta}$ increase, the slider will eventually decelerate before reaching slip instability. For the system to reach instability, we need both $\dot{V} > 0$, $\dot{\theta} < 0$ and $\ddot{\theta} < 0$. The state acceleration is given by (taking the time derivative of (2), and using expression (10) of $\dot{V}$, and expression (2) of $\dot{\theta}$)

$$\ddot{\theta} = \frac{-\dot{\theta}V - \theta\dot{V}}{D_c} = \frac{\dot{\theta}V}{D_c}\left(\frac{B}{A} - 1 - \frac{kD_c}{A\sigma}\right) + \frac{kV}{A\sigma}. \qquad (16)$$

The condition for $\ddot{\theta} < 0$ thus corresponds to $\dot{\theta} < 1/(1 - k_c/k)$ or to a friction larger than $\mu_l(V)$ (8). We thus recover the condition for instability derived by *Ranjith and Rice* [1999] using a nonlinear analysis of the rate-and-state friction law with the aging law and for negligible loading rate.

[23] The friction at the stability limit (8) for $A < B$ and $k < k_c$ is larger than the condition for initial acceleration (15) of the slider. Between these two values, there is thus a range of parameters for which we observe slow earthquakes, followed by a classic afterslip relaxation, in both the velocity-strengthening or velocity-weakening regimes.

[24] If we include a stressing rate $\dot{\tau}$, accelerations are possible for a stiffness larger than k_B. If slip rate is very large so that $\dot{\theta}/\theta$ in (11) can be replaced by $-V/D_c$, the condition for acceleration (11) becomes [*Dieterich*, 1992]

$$k < k_B + \dot{\tau}/V. \qquad (17)$$

With a positive loading rate, slow earthquakes can thus occur even for $\mu < \mu_{ss}(V)$ and $k > k_B$, because in that case
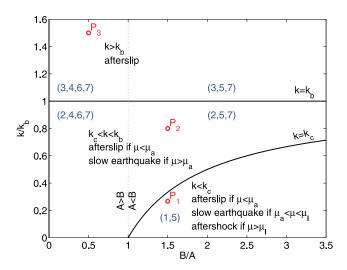

Figure 1. Different postseismic behaviors as a function of B/A and k/k_B. Points labeled P_1, P_2, and P_3 refer to parameter sets used in Figure 5. Numbers in parentheses correspond to the asymptotic regimes described in section 3 and Table 2 which can be observed for each range of parameters k/k_B and A/B.

the threshold for acceleration is smaller than $\mu_a(V)$, and can even be below steady state if slip rate is lower than the loading rate. With the aging law, purely periodic slow earthquakes occur only at the stability transition, for $k = k_c$ and $B > A$. In contrast, the slip law can produce periodic events for a finite range of model parameters, with $k < k_c$ and $B > A$ [*Gu et al.*, 1984].

[25] In summary, the existence of instabilities is controlled by the stiffness k, by the ratio B/A and by the stress level. Instabilities, with slip rate increasing up to infinity, are possible only for $k < k_c$, while k_B controls the existence of slip accelerations. But in order to produce slip instabilities or accelerations, we also need large enough stresses. The minimum stress required for accelerations and instabilities are defined by (15) and (8), respectively. Figure 1 illustrates the different postseismic behaviors as a function of B/A and k/k_B. Figure 2 represents the same results as a function of B/A and $|k/k_c|$. Figure 3 illustrates the trajectories of the system in a diagram of friction versus slip rate, in the different stress regimes, for simulations with $A < B$, $k < k_c$ and without loading rate. Depending on the value of the friction relative to $\mu_a(V)$ and $\mu_l(V)$, we get either afterslip, slow earthquakes, or aftershocks.

2.4. Slow Earthquakes

[26] *Rice and Gu* [1983] and *Gu et al.* [1984] analyzed analytically and numerically a one degree of freedom slider block model and found that this model can produce slow slip transients that are similar to the slow earthquakes or "creep events" observed in nature. In the model, slow earthquakes occur close to the stability transition either as individual events triggered by a stress change or as spontaneous periodic events. Slow earthquakes can be triggered by a main shock if it loads the fault above steady state ($\mu > \mu_a$). But slow earthquakes can also be produced by the tectonic stress. With a positive loading rate, slow earthquakes can occur even for $k > k_B$ and for stress smaller than
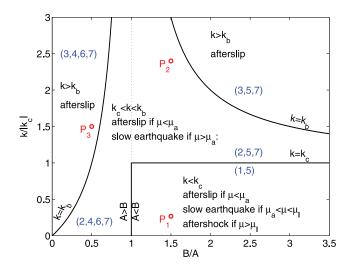
Figure 2. Same as Figure 1 but using the critical stiffness for acceleration k_B for normalizing k.

than steady state. These slow earthquakes can occur individually, or as a sequence of events with interevent time and amplitude decreasing with time, for any choice of B/A and stiffness.

[27] In nature, slow earthquakes have been observed in subduction zones [*Szeliga et al.*, 2008], along the San Andreas fault [*Scholz et al.*, 1969; *Wesson*, 1988; *Bilham*, 1989; *Bodin et al.*, 1994; *Langbein et al.*, 2006], and at Hawaii on a shallow fault [*Segall et al.*, 2006]. Slow earthquakes may also accommodate most of the deformation along ridge transform faults [*Boettcher and Jordan*, 2004]. They occur generally above [*Bilham*, 1989] or below [*Dragert et al.*, 2001; *Mitsui and Hirahara*, 2006] the seismogenic zone. Slow earthquakes in the subduction zones occur sometimes regularly, often irregularly, with a

period of the order of a year. *Szeliga et al.* [2008] analyzed 34 slow events in the Cascadia subduction zones. While events occur at regular time intervals in some areas, other zones do not show any clear periodicity, and the size of successive slow events in the same zone may be very different.

[28] There have been also observations of slow earthquakes triggered by an earthquake, in California [*Scholz et al.*, 1969; *Wesson*, 1988; *Bilham*, 1989; *Bodin et al.*, 1994; *Langbein et al.*, 2006] and after the 1995 $M = 8.1$ Chile earthquake [*Pritchard and Simons*, 2006]. Following the 1987 Superstition Hill earthquake, or the 1966 and 2004 Parkfield earthquakes, afterslip on parts of the fault occurred as sequences of creep events of similar amplitude and increasing interevent times [*Scholz et al.*, 1969; *Wesson*, 1988; *Bilham*, 1989; *Langbein et al.*, 2006].

[29] Many studies have recently used the rate-and-state friction law to model slow earthquakes [*Boatwright and Cocco*, 1996; *Belardinelli*, 1997; *Reinen*, 2000; *Du et al.*, 2003; *Shibazaki and Iio*, 2003; *Yoshida and Kato*, 2003; *Hirose and Hirahara*, 2004; *Liu and Rice*, 2005, 2007; *Lowry*, 2006; *Mitsui and Hirahara*, 2006; *Perfettini and Ampuero*, 2008]. Most studies used one or a few slider blocks, but more recent studies use a 2-D or 3-D continuous fault model [*Shibazaki and Iio*, 2003; *Hirose and Hirahara*, 2004; *Liu and Rice*, 2005, 2007; *Perfettini and Ampuero*, 2008]. Although the simple rate-and-state friction law is able to produce slow earthquakes, several studies used a more complex law, with friction parameters A and B function of slip rate [*Reinen*, 2000; *Shibazaki and Iio*, 2003], so that the fault is velocity weakening at slow slip velocity and velocity strengthening at large slip rate, or with two state variables [*Du et al.*, 2003], or a complex dependence of friction and state rate on slip rate [*Belardinelli*, 1997]. *Belardinelli* [1997] also introduced time-dependent changes in the model parameters in order to model loga-
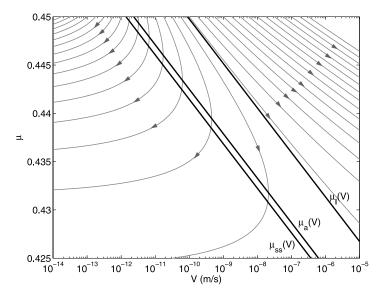

Figure 3. Trajectories for numerical simulations of a slider block with $B/A = 1.2$ and $k/k_c = 0.5$ (grey curves). Black curves show the steady state friction and the boundaries for acceleration $\mu_a(V)$ and instability $\mu_l(V)$. Trajectories starting with $\mu < \mu_a(V)$ have a slip rate continuously decreasing with time. Between $\mu_a(V)$ and $\mu_l(V)$ the system produces slow earthquakes, and above $\mu_l(V)$ slip rate continuously increases.

rithmic increase of interevent time between creep events triggered by a main shock. Numerical simulations with continuous faults models have been able to model the nucleation and propagation of slow earthquakes, the stress heterogeneity, and interactions between earthquakes and slow events, including realistic changes in the model parameters A, B and σ and $\dot{\tau}_l$ with depth [*Hirose and Hirahara*, 2004; *Rubin and Ampuero*, 2005; *Liu and Rice*, 2005, 2007; *Perfettini and Ampuero*, 2008]. Most studies found slow earthquakes occurring on velocity-strengthening faults [*Perfettini and Ampuero*, 2008] or close to the stability transition for $B \approx A$ [*Boatwright and Cocco*, 1996; *Liu and Rice*, 2005, 2007]. But a few models produced slow earthquakes with $A < B$ and $k \geq k_c$ [*Yoshida and Kato*, 2003; *Mitsui and Hirahara*, 2006; *Lowry*, 2006] or even for $A < B$ and $k < k_c$ in the source zone of ordinary earthquakes due to stress heterogeneity [*Hirose and Hirahara*, 2004]. The possibility that slow earthquakes could occur on velocity-weakening faults was also raised by *Rubin and Ampuero* [2005], who showed that nucleation do not localize on small patches if A is sufficiently close to B. Slow earthquakes then happen if the fault is not large enough to support the full nucleation stage.

[30] Most studies performed only numerical simulations. Analytical studies demonstrated the existence of periodic slow earthquakes at the stability limit (for $k = k_c$ and $A < B$) for a single degree of freedom slider block with constant loading velocity [*Gu et al.*, 1984]. The oscillations of slip rate decay or grow in amplitude when stiffness is either slightly smaller or larger than k_c. An exact expression for the slip rate as a function of friction for a constant load point (or for a constant loading rate but with $k = k_c$) was obtained by *Gu et al.* [1984] for the slip law and by *Ranjith and Rice* [1999] for the aging law. *Perfettini and Ampuero* [2008] compared analytical study of a single slider block system with numerical simulations of multidimensional fault planes. They found approximate expressions for the amplitude of the maximum slip rate and the nucleation time.

2.5. Steady State Approximation for Afterslip

[31] Previous studies have used the rate-and-state friction law to model afterslip, assuming the fault is close to the steady state regime [*Scholz*, 1990; *Marone et al.*, 1991; *Wennerberg and Sharp*, 1997; *Marone*, 1998; *Schaff et al.*, 1998; *Hearn et al.*, 2002; *Hearn*, 2003]. Other studies used a rate-dependent friction law, that is equivalent to the expression for steady state friction in the rate and state law (6) by replacing (A-B) by another positive parameter [*Montési*, 2004; *Perfettini and Avouac*, 2004, 2007; *Perfettini et al.*, 2005; *Langbein et al.*, 2006; *Johnson et al.*, 2006; *Hsu et al.*, 2006]. They suggested that afterslip is produced within velocity-strengthening ($A > B$) parts of the fault, below or above the seismogenic zone (where $A < B$ to produce earthquakes). In these zones, there is a slip deficit after an earthquake, and thus an increase in Coulomb stress, which is relaxed during afterslip. The steady state approximation assumes that healing is extremely rapid so that friction recovers very quickly its steady state. It requires very small values of D_c, much smaller than the amplitude of afterslip.

[32] With the steady state approximation $\dot{\theta} \approx 0$, and without loading stress rate ($\dot{\tau}_l = 0$), afterslip increases logarithmically with time [*Scholz*, 1990; *Marone et al.*, 1991]

$$\delta = V_0 t_0 \ln\left(\frac{t}{t_0} + 1\right), \tag{18}$$

where V_0 is the initial slip speed and

$$t_0 = \frac{\sigma(A - B)}{kV_0} \tag{19}$$

is a characteristic time for afterslip. Slip speed given by

$$V = \frac{V_0}{1 + t/t_0}, \tag{20}$$

decreases as the inverse of time for $t > t_0$.

[33] We can test the limit of validity of equation (18) by injecting the solution for the slip speed (20) into the evolution law (2). If $\dot{\theta} = 0$, then (2) reduces to

$$\theta = \frac{D_c}{V} = \frac{D_c(1 + t/t_0)}{V_0}. \tag{21}$$

Taking the time derivative of (21), we find that the state-rate obeys

$$\dot{\theta} = D_c/t_0 V_0 = k/k_c. \tag{22}$$

This shows that the steady state approximation (18) works only for very small stiffness $k \ll k_c$. This requirement is equivalent to assuming a very small critical slip distance, because $k_c \sim 1/D_c$.

[34] Decrease in velocity with time in the evolution law (2) has to be balanced by an increase in state and/or state rate. Therefore, the steady state regime $\dot{\theta} = 0$ can be reached only at constant slip rate [*Rice and Gu*, 1983]. Nevertheless, application of expression (18) provides a very good fit to afterslip data, with however significant discrepancies [*Wennerberg and Sharp*, 1997; *Montési*, 2004]. To better explain the data, *Wennerberg and Sharp* [1997] have used a more complex form of equation (1). They have also suggested to introduce a second state variable in (1), in order to explain apparent negative values of A obtained when inverting afterslip data, and to explain the transition between aseismic and seismic slip during the earthquake cycle.

[35] *Perfettini and Avouac* [2004] and *Montési* [2004] introduced a nonzero loading rate V_l in order to better fit GPS data. The slip rate then obeys

$$V = \frac{V_0}{(1 - V_0/V_l)e^{-\frac{tkV_l}{A\sigma}} + V_0/V_l}. \tag{23}$$

Few studies checked the validity of the steady state assumption and verified that $\dot{\theta}$ in the evolution law (2) is indeed negligible during afterslip. *Marone et al.* [1991] performed numerical simulations without the quasi-static approximation (6), which were in good agreement with the analytical solution (18) for a few cases. *Perfettini and Avouac* [2007] and *Perfettini and Ampuero* [2008] also

performed numerical simulations and analytical study to test the steady state approximation. They found that for times larger than the characteristic time t_0 defined by (19), the steady state friction law (23) is very close to the full rate-and-state law. At earlier times, they observed a transient slip acceleration because they considered both very small stiffness $k \ll k_B$ and large initial stress, well above steady state. Assuming $D_c = 1 \ \mu m$, they estimated t_0 to be equal to 9 h. This suggests that the steady state approximation was pertinent for their analysis of Landers postseismic displacement, which started to be observed 12 days after the main shock. However, this approximation becomes incorrect at shorter time scales, or at times smaller than 100 years if a larger value of $D_c = 10 \ cm$ is used, as suggested by recent friction experiments [*Di Toro et al.*, 2004; *Hirose and Shimamoto*, 2005] or by seismic inversion [*Ide and Takeo*, 1997].

2.6. Afterslip and Fault Zone Rheology

[36] Most afterslip generally occurs below or above the seismogenic zone [*Marone et al.*, 1991; *Hsu et al.*, 2006]. These areas are expected to be velocity strengthening from the dependence of B-A with temperature and normal stress estimated in laboratory experiments. But there are also observations suggesting that some afterslip can occur along strike the rupture zone [*Melbourne et al.*, 2002; *Pritchard and Simons*, 2006; *Chlieh et al.*, 2007], or even within the rupture area [*Miyazaki et al.*, 2004], and can be associated with aftershocks [*Miyazaki et al.*, 2004]. To explain these observations within the steady state approximation, we need to invoke small-scale spatial or temporal variations of the friction parameters A or B [*Miyazaki et al.*, 2004; *Wennerberg and Sharp*, 1997].

[37] *Perfettini and Ampuero* [2008] argued that afterslip on velocity-weakening faults may occur only over very narrow zones, of size smaller than about 1 km, so that $k > k_B$, otherwise slip rate would increase toward instability. We do not agree with this argument, because we have shown in the previous section that the condition $k < k_B$ is not sufficient to produce slip accelerations, we also need a large enough stress. If initial stress is not (much) larger than steady state, even very large faults (with $k \ll k_B$) produce afterslip that decays roughly as a power law of time.

[38] *Miyazaki et al.* [2004] attempted to distinguish between velocity-weakening and velocity-strengthening behavior for different parts of the fault that slipped after the 2003 Tokachi-oki earthquake. They inverted afterslip and stress changes on the fault from GPS data. They found that, within the rupture area, slip rate and stress initially decrease with time. But then stress increases while slip velocity continues to decrease. For other parts of the fault around the rupture area, stress decreases roughly linearly with the log of the slip rate, as expected with the steady state approximation (6). *Miyazaki et al.* [2004] interpreted these results as evidence for velocity-weakening (unstable) behavior within the rupture area, and velocity-strengthening regime around the main shock rupture. We suggest that the different behavior between the rupture area and surrounding regions may alternatively arise from different stress histories: stress increases within the rupture area because it is reloaded by surrounding region, where afterslip is larger.

[39] *Marone et al.* [1991] also evoked the possibility that afterslip may be produced by unstable faults, but noted that "for a fault that exhibits only velocity-weakening behavior, the steady state frictional resistance decreases with slip velocity, eliminating the stress transient needed to drive afterslip." However, it is possible to produce significant afterslip starting from friction at or below the steady state with $A < B$. In addition, earthquake rupture is more complex than with single degree of freedom systems. There may be parts of the fault where stress transfers during dynamic rupture propagation can produce stress concentration, so that stress can be locally larger than its steady state value after a main shock. Also, in higher dimensions, stiffness itself becomes a dynamical variable through the evolution of slipping patches, which can affect in significant ways the evolution of various phases. This has been shown to be the case for nucleation in quite thorough 2D treatments by *Rubin and Ampuero* [2005]. Examining the phase space of behaviors, which we now turn to, in a higher dimensional context will thus be of additional interest.

3. Evolution of Slip and State Variable With Time

[40] We have performed numerical simulations and analytical study of the slider block model with a constant loading rate. There is no exact solution, but several asymptotic expressions can be found for stress either much smaller or much larger than steady state, or for state rate close to its long-time value $\dot{\theta}_l$ if $V \gg V_l$ and $A > B$. For each regime, we show the expressions for the slip, slip rate, state, and friction as a function of time. We found several regimes that produce an Omori law decay of slip rate with time $V \sim t^{-p}$ with different exponent values. Most solutions have already been published previously; we have essentially synthesized scattered results derived by others [*Scholz*, 1990; *Dieterich*, 1992; *Montési*, 2004; *Rubin and Ampuero*, 2005]. Some of these results were derived to describe earthquake nucleation, but may describe afterslip as well. The only new result has been obtained for the case of a constant state-rate, but the slip history in that regime is identical to that of the steady state approximation. By gathering together these different solutions in different regimes, and showing how they link together, we show more generally the variety of ways the system evolves for different B/A, k and stress.

[41] Figures 1 and 2 and Table 2 summarize the possible behaviors in each range of parameters, as a function of stiffness and B/A. Figure 4 illustrates the evolution of state rate for different values of B/A, for a fixed value of stiffness equal to $0.4k_b$. It emphasizes the role of initial stress in controlling the postseismic behavior. Figure 5 shows the temporal evolution of velocity, state variable, and friction, for numerical simulations with different values of B/A, stiffness, and initial stress, and compares the numerical results with analytical solutions.

3.1. Solution for Stress Much Larger Than Steady State

[42] *Dieterich* [1992] derived an asymptotic solution for large slip rate such that $\mu(V) \gg \mu_{ss}(V)$. He used this solution to describe the nucleation phase preceding slip instabilities, but the same expression can also be used to describe

Table 2. Analytical Approximations for the Evolution of State and Slip With Time

	Regime[a]						
	1	2	3	4	5	6	7
condition	$k < k_c$	$k_c < k < k_B$	$k > k_B$	$A > B$	$A < B$	$A > B$	$k > k_c$
approx.	$\mu \gg \mu_{ss}(V)$	$\mu \gg \mu_{ss}(V)$	$\mu \gg \mu_{ss}(V)$	$\mu \ll \mu_{ss}(V)$	$\mu \ll \mu_{ss}(V)$	$\mu \approx \mu_l(V)$	$\mu \approx \mu_{ss}(V)$
V	$V \nearrow$[b]	$V \nearrow$	$V \searrow$	$V \searrow$	$V \searrow$	$V \searrow$	$V = V_l$
$\dot\theta$	$\dot\theta \searrow$	$\dot\theta \nearrow$	$\dot\theta \nearrow$	$\dot\theta \searrow$	$\dot\theta \nearrow$	$\dot\theta \approx \dot\theta_l$	$\dot\theta = 0$
p				1	B/A	B/A	1
evolves toward	$V = \infty$	6 if $A > B$ 5 if $A < B$	7	6 if $A > B$ 5 if $A < B$	7 if $k > k_c$ 1 if $k < k_c$	7	

[a]Regimes are 1, instability; 2, transient slip; 3–6, afterslip; 7, steady state.
[b]Arrows indicate whether a variable is increasing or decreasing with time.

postseismic relaxation or the nucleation phase of slow earthquakes. It may be applied as well for velocity-weakening or velocity-strengthening faults. If friction is much larger than steady state, then state-rate is much smaller than zero and the evolution law (2) reduces to [Dieterich, 1992]

$$\dot\theta = -V\theta/D_c. \tag{24}$$

The solution for the displacement is (equations (22) and (23) of Dieterich [1992] with different variables and notations)

$$\delta = V_0 t_1 \ln\left[1 - \frac{t_a}{t_1}\left(1 - e^{t/t_a}\right)\right] \text{ for } \dot\tau_l \neq 0, \tag{25}$$

$$\delta = V_0 t_1 \ln(1 + t/t_1) \text{ for } \dot\tau_l = 0, \tag{26}$$

$$t_1 = \frac{A\sigma}{V_0(k - k_B)}, \tag{27}$$

$$t_a = A\sigma/\dot\tau_l. \tag{28}$$

[43] The corresponding expressions for the slip rate are (equations (24) and (25) of Dieterich [1992])

$$V = \frac{V_0}{\left(1 - \frac{t_a}{t_1}\right)e^{-t/t_a} + \frac{t_a}{t_1}} \text{ for } \dot\tau_l \neq 0, \tag{29}$$

$$V = \frac{V_0}{1 + t/t_1} \text{ for } \dot\tau_l = 0. \tag{30}$$

The solution of (24) for the state variable is [Dieterich, 1992]

$$\theta = \theta_0 \exp(-\delta/D_c), \tag{31}$$

and the state-rate obeys

$$\dot\theta = -\frac{V\theta_0}{D_c}\exp(-\delta/D_c). \tag{32}$$

[44] If loading rate is negligible, we can rewrite expression (1) for μ using (26, 27, 30, and 31)

$$\mu = \mu_0 + \frac{A}{1 - k_B/k}\ln\frac{V}{V_0}. \tag{33}$$

The trajectories of the system thus follow straight lines in a diagram μ as a function of $\ln(V)$, but with a slope different from the value A-B characteristic of the steady state regime (6).

3.1.1. Regime 1: Case $k < k_c$

[45] The condition $k < k_c$ requires $A < B$ and $k < k_B$, so the characteristic time t_1 defined by (27) is negative. Expressions (29 and 30) thus describe a power law singularity of the slip rate. It can be used to model aftershocks triggered by a static stress change. The time at which slip rate is infinite is given by (equations (26) and (27) of Dieterich [1992]):

$$t_i = -t_a \ln(1 - t_1/t_a) \text{ for } \dot\tau_l \neq 0, \tag{34}$$

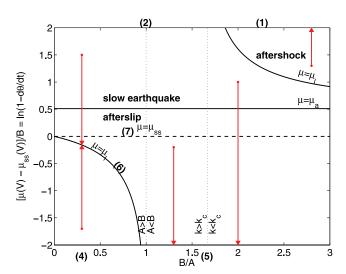$$t_i = -t_1 \text{ for } \dot\tau_l = 0. \tag{35}$$

Figure 4. Friction or state rate relative to steady state as a function of B/A for $k = 0.4k_B$ and $\dot\tau_l = 0$. Also shown are limits for acceleration and instability and examples of trajectories in this space (arrows) in the absence of tectonic loading. Numbers in parentheses refer to asymptotic solutions described in section 3 and Table 2.
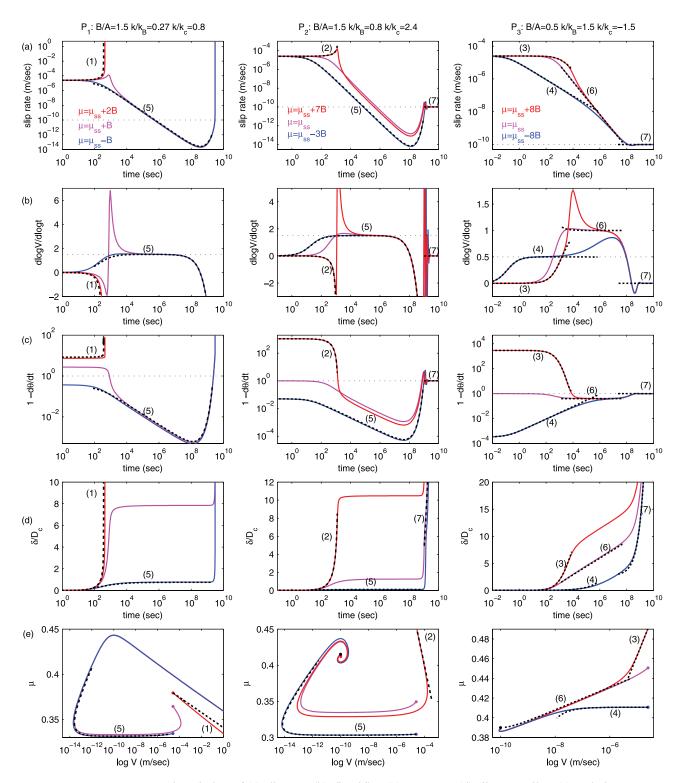
Figure 5. Temporal evolution of (a) slip rate, (b) $d\ln V/d\ln t$, (c) state rate, (d) slip, as well as (e) variation of friction with slip rate for numerical simulations with different choices of parameters B/A and k (see values at the top and in Figures 1 and 2) and with $A = 0.01$, $D_c = 0.01$ m, and $\sigma_n = 100$ MPa, and a loading rate $V_l = 10^{-10}$ m/s. In each plot, each curve corresponds to a different value of initial friction (see values in Figure 5a). In Figure 5a the dotted curve shows the loading rate. In Figure 5b the dotted curve shows the ratio $B = A$. In Figure 5c the dotted curve is the steady state $\mu = 0$. The dashed curves are asymptotic analytical solutions. The regime number is indicated close to each curve, and all regimes are summarized in Table 2.

In this regime, state-rate decreases with time, so that expressions (29 and 30) can be used until the singularity at $t = t_i$. Of course, for real faults slip rate does not exceed about 1m/s during dynamic ruptures, so we should not use our model for very large slip rate because it does not include inertial effects.

3.1.2. Regime 2: Case $k_c < k < k_B$

[46] This regime may apply as well for velocity-weakening or velocity-strengthening faults. Expressions (29 and 30) describe the nucleation phase of a slow earthquake. As time increases, state rate increases and the approximation (24) is no more valid. Nevertheless, expressions (34 and 35) give a correct estimation of the time of the maximum slip rate.

3.1.3. Regime 3: Case $k > k_B$

[47] For $k > k_B$, the characteristic time t_1 defined by (27) is positive. This regime describes afterslip, with a constant slip rate for $t \ll t_1$, followed by a power law decrease $V \sim 1/t$ for $t_1 \ll t \ll t_a$ and as long as friction is well above steady state. The characteristic time t_1 is inversely proportional to initial slip rate: the faster the fault slips, the shorter is the time interval when the fault starts to slip. State-rate is constant for $t \ll t_1$ then increases with time.

[48] For large times, expression (29) predicts that $V \approx V_l/(1 - k_B/k)$ for $t \gg t_a$; that is, a value larger than the loading point velocity. Of course, the long-time slip rate is equal to the loading velocity. But at constant slip rate, state-rate is zero so the approximation $\dot{\theta} \ll 0$ used to derive equations (29 and 30) does not hold anymore. So expressions (29 and 30) cannot be used to describe the relaxation of slip rate toward the loading rate, but are only valid as long as $V \gg V_l$.

[49] We found in numerical simulations that, depending on B/A and V_0, state rate either continuously increases toward steady state, or crosses the origin and stays above zero for $t \ll t_a$. After a time much larger than the nucleation time, the system reaches steady state ($V = V_l$ and $\dot{\theta} = 0$).

3.2. Solution for Stress Much Smaller Than Steady State

[50] When stress is much smaller than steady state friction, we have $\dot{\theta} \approx 1$, so $V \ll D_c/\theta$ and

$$\theta \approx \theta_0 + t. \tag{36}$$

Because slip rate is small, we can neglect elastic interactions $k\delta$ in (4). The rate-and-state friction law thus becomes

$$\frac{\dot{\tau}_l t}{\sigma} \approx A \ln \frac{V}{V_0} + B \ln\left(\frac{1+t}{\theta_0}\right). \tag{37}$$

The solution of (37) for the slip rate was derived by *Rubin and Ampuero* [2005]

$$V \approx \frac{V_0 e^{t/t_a}}{(1 + t/\theta_0)^{B/A}}. \tag{38}$$

The characteristic time θ_0 in (38) is always positive, so the slip rate decays as a power law with time for $\theta_0 \ll t \ll t_a$. Expression (38) can thus be used to model afterslip, and may explain why Omori exponent for slip rate is sometime

found to be different from 1. This solution for the slip rate is identical to that derived by *Helmstetter et al.* [2004] to model landslides displacement, for the special case $k = 0$ and $V_l = 0$.

[51] An explicit expression for the slip can only be found for $t \ll t_a$ (negligible loading rate)

$$\delta \approx \frac{V_0 \theta_0}{B/A - 1}\left[1 - (1 + t/\theta_0)^{1-B/A}\right]. \tag{39}$$

Putting expressions (36) for θ and (38) for V into the evolution law (2) we get

$$\dot{\theta} \approx 1 - \frac{\theta_0 V_0}{D_c} e^{t/t_a}\left(1 + \frac{t}{\theta_0}\right)^{1-B/A}. \tag{40}$$

In this regime, elastic interactions are negligible so that μ decreases very slowly with V.

3.2.1. Regime 4: Case $A > B$

[52] In the velocity-strengthening regime $1 - B/A > 0$ so the state-rate (40) decreases with time; that is, the stress increases toward steady state. However, we found in the numerical simulations that state rate does not continuously decrease toward 0. Rather, friction evolves toward $\mu_l(V) < \mu_{ss}(V)$, where $\mu_l(V)$ is defined by (8), and the exponent of the power law decay of slip rate versus time changes from B/A to 1 (see regime 6 below).

3.2.2. Regime 5: Case $A < B$

[53] In this case, state-rate increases with time for $t \ll t_a$ up to a maxima at $t \approx t_a$. Slip rate decays as a power law for $t \ll t_a$ and reaches a minima for $t >\approx t_a$, which can be much smaller than the loading rate; then it increases quasi exponentially with time [*Rubin and Ampuero*, 2005]. When state-rate becomes negative, the approximation $\dot{\theta} \approx 1$ is no more valid. If $k < k_c$ the system evolves toward a slip instability that can be modeled with regime 1. If $k > k_c$, the system evolves toward steady state (regime 7), with possible oscillations around steady state.

3.3. Regime 6: Solution for Constant State Rate

[54] We found in numerical simulations, in the absence of loading rate and for $A > B$, that the system does not evolve toward steady state but toward a constant state rate equal to

$$\dot{\theta}_l = \frac{1}{1 - k_c/k}. \tag{41}$$

This gives a state variable increasing linearly with time

$$\theta = \theta_0 + \dot{\theta}_l t. \tag{42}$$

We could find an explicit solution only for negligible loading rate $V \gg V_l$. Putting expression (42) of θ and (41) of $\dot{\theta}$ into the rate-and-state friction law (2) with $\dot{\tau}_l = 0$ gives the following solution for the slip rate and for the slip

$$V = \frac{V_0}{1 + t/t_0}, \tag{43}$$

$$\delta = V_0 t_0 \ln(1 + t/t_0), \tag{44}$$

$$t_0 = \frac{\theta_0}{\dot{\theta}_l} = -\frac{k_c D_c}{k V_0} = \frac{(A - B)\sigma}{k V_0}. \tag{45}$$

These expressions for slip rate, slip, and state variable satisfy the rate-and-state friction law (1) with $\dot{\tau}_l = 0$. This solution for the slip and slip rate is identical to the steady state approximation for afterslip derived by *Scholz* [1990], but, in contrast with the steady state approximation, the state-rate is significantly different from zero, and stress is lower than steady state. Afterslip in this regime is thus associated with slow healing of the fault. If k is much smaller than k_c, i.e., for small D_c or long faults with $L \gg L_c$, the healing rate $\dot{\theta}_l$ defined by (41) is almost zero as assumed in the steady state approximation. As for regime 3, the characteristic time t_0 scales with initial slip rate.

[55] In the presence of a constant loading rate, this solution is valid as long as $V \gg V_l$, i.e., for times much smaller than t_a. At larger times, V evolves toward V_l and $\dot{\theta}$ decreases toward zero. In most cases, we found numerically that V decreases below V_l then increases back to V_l, while the steady state approximation (23) predicts a smooth decay toward V_l.

[56] Using (8) and (42), expression (14) for friction gives

$$\mu = \mu_0 + (A - B)\ln\frac{V}{V_0} + B\ln(1 - \dot{\theta}_l) = \mu_l(V). \qquad (46)$$

The trajectories of the system thus follow straight lines in a diagram μ as a function of $\ln(V)$ that are parallel to the steady state regime (6).

3.4. Regime 7: Steady State

[57] At steady state $\dot{\theta} = 0$ the evolution law reduces to

$$\theta V = D_c. \qquad (47)$$

Because $\dot{\theta} = 0$, the state variable is constant $\theta = \theta_0$, which implies from (47) that $V = D_c/\theta_0$ is also a constant. The only solution of the rate-and-state law (1) and (4) with constant V and θ, and for $k > 0$, is to have slip rate equal to the loading rate [*Rice and Gu*, 1983].

3.5. Summary of Analytical Results

[58] Figures 1 and 2 and Table 2 summarize the possible behaviors in each range of parameters, as a function of stiffness and B/A. In the absence of loading rate, friction evolves toward $\mu_l(V)$ for $A > B$. If $A < B$, friction becomes either much larger than $\mu_{ss}(V)$ if $k < k_c$ (slip rate singularity) or much lower than steady state if $k > k_c$ (decreasing slip rate).

[59] If we include a constant loading rate V_l, slip rate evolves toward V_l and friction reaches steady state at large times $t \gg t_a$ when $k > k_c$. In the case $k < k_c$, the system evolves toward a slip singularity even if the initial stress was below $\mu_l(V)$.

[60] At short times $t \ll t_a$, we found several solutions for the slip rate of the form

$$V = \frac{V_0}{(1 + t/t^*)^p}, \qquad (48)$$

where the exponent p is either smaller, equal or greater than 1 depending on the model parameters, and t^* is a characteristic time, which depends on the initial conditions and on the friction law parameters. In regime 3, we have $p = 1$ and $t^* = t_1$. In regime 6, we found $p = 1$ and $t^* = t_0$. In regimes 4 or 5, $p =$

B/A and $t^* = \theta_0$. Generally, the system evolves from one regime to another one with time, so that the exponent p can either increase or decrease with time. Depending on B/A, k/k_B, and μ_0, total afterslip can be either much smaller or larger than D_c. Even for seismogenic faults (with $k < k_c$), total afterslip can be much larger than D_c.

[61] The steady state approximation for slip rate (20) introduced by *Scholz* [1990] is identical to our solution in regime 6. However, in this regime the state-rate is nonzero but equal to $\dot{\theta}_l$, and stress is lower than steady state. The behavior of the complete rate-and-state law is by far more complex than described by the steady state approximation. The complete rate-and-state friction law reduces to the steady state solution (20) only for $A > B$, $k \ll |k_c|$ and at large times (or for very small D_c) [*Perfettini and Avouac*, 2007]. Because of its simplicity and of its rather good performance in fitting afterslip data, the use of expression (20) for modeling afterslip data is legitimate. But it should be renamed, e.g., "rate-dependent friction law" as the term "steady state approximation" is incorrect. Also, the parameters of the rate-dependent friction law should not be compared to those of the complete rate-and-state friction law, because several regimes can produce a slip rate similar to the rate-dependent friction law but for different values of the friction law parameters.

4. Fitting Afterslip Data

4.1. Introduction

[62] Several studies have attempted to measure A or A-B, and to distinguish between the stable and unstable regimes from the evolution of stress with slip rate during afterslip. *Miyazaki et al.* [2004] have mapped the coseismic and postseismic slip produced by the 2003 Tokachi-oki earthquake, as well as the change in shear stress on the fault, by inverting GPS time series. Most afterslip occurred around the rupture area, mostly downdip. Within these zones, the stress velocity paths approximately follow $d\tau/d \ln(V) = 0.6$ MPa. They interpreted this result as an evidence that the main afterslip regions are velocity strengthening. They assumed that stress is at steady state, and suggested that $(A$-$B)\sigma = 0.6$ MPa. But there are other cases that produce a linear decrease of friction with $\ln(V)$. The fault may be in the first regime, corresponding to a stiff fault with $k > k_B$ and $\mu \gg \mu_{ss}(V)$. In this case the slope $d\tau/d \ln(V)$ would be equal to $A/(1 - k_B/k)$ instead of A-B, and we cannot distinguish between the velocity-weakening or velocity-strengthening regimes. *Miyazaki et al.* [2004] also found significant afterslip within the rupture area, but with less slip than the surrounding zones, of the order of 0.1 m instead of 0.5 m downdip of the rupture zone. In this zone, stress decreases a little at short times, and then reloads, because afterslip is larger in the surrounding areas. They suggest that this behavior is similar to that of a single degree of freedom slider block model with a constant loading rate in the velocity-weakening regime.

[63] *Hsu et al.* [2006] applied the same method to the 2005 Nias earthquake, and obtained a similar result. They observed extensive afterslip updip from the main shock and a lack of substantial overlap between seismogenic and aseismic regions. Aftershock zones correspond to the transition between regions of coseismic and aseismic slip. In the regions of large afterslip, stress decreases roughly linearly

with $\ln(V)$, with a slope $d\tau/d\ln(V) \approx 0.2$ MPa at short times, but much smaller for times larger than 100 days. In the areas of smaller afterslip, shear stress increases a little with time, because these zones are reloaded by surrounding slipping areas. *Hsu et al.* [2006] nevertheless measure $A\sigma$ from the slope $d\tau/d\ln(V) \approx -0.02$ MPa, giving unphysical negative values for A.

[64] We have fitted a 1-D slider block model with the rate-and-state law to the postseismic data of three recent earthquakes, the 2000 $M_w 8$ Denali earthquake [*Freed et al.*, 2006a, 2006b], the 2004 $M_w 6$ Parkfield earthquake [*Langbein et al.*, 2006], and the 2005 $M_w 8.7$ Nias event [*Hsu et al.*, 2006]. For each data set, we have compared the full rate-and-state friction law (with constant loading rate and using the aging evolution law) with the rate-dependent friction law (equation (6) with $A > B$) and with an empirical Omori law decay of slip rate superposed to a constant loading rate. An exponential relaxation with time was also tested, but, for most cases, the fit was not as good as the other laws. We have used GPS data for all earthquakes and also creepmeter data for Parkfield. In all cases, we have used only the norm of the horizontal displacement, in order to decrease the number of data sets. Because it is difficult to separate coseismic and postseismic slip, and because our simple model without inertial effects cannot describe the early afterslip, we have added an adjustable offset to each data set. In each fit, this offset is estimated so that the average slip of the model matches that of the data.

4.2. Afterslip Data

4.2.1. GPS Data for Parkfield

[65] We analyzed the GPS data of *Langbein et al.* [2006], which is available on the Web as an electronic supplement. *Langbein et al.* [2006] analyzed postseismic displacement from 100 s through 9 months following the main shock. The points PKDB, CARH, and LOWS were rejected from the analysis because of their smaller amplitude, and we analyzed the 10 remaining points. The displacement is estimated relative to a site farthest from the fault, CRBT. During the first 12 h after the main shock, there is one measure of displacement for each minute. The sampling rate decreases to one point per 30 min during the first 20 days and then to one point per day. We analyzed all data points without resampling or additional smoothing.

4.2.2. Creepmeter Data for Parkfield

[66] We also analyzed the creepmeter data provided by *Langbein et al.* [2006]. The creepmeter uses an invar wire to measure the change in distance between two piers located on either side of the surface trace of the fault. The measurements are made every 10 min. The sensor can resolve distance changes of less than 0.05 mm. We used nine sites on the San Andreas fault analyzed by *Langbein et al.* [2006], rejecting site xsc1 which had little afterslip and site xpk1 which broke during the earthquake. At many sites, the coseismic slip exceeded the 25-mm range of the instrument. In most cases, the invar wire was stretched but not broken, which allowed the instrument to be manually reset within 4 days after the main shock. Therefore, sites crr1, xmd1, xta1, xva1, and xmm1 have no data between about 0.1 and 2 days. Measurements for site wkr1 started about 2 days after the main shock. The displacement was resampled using a logarithmic time scale, in order to reduce the

number of points. Also, because the density of measures is uniform in $\log(t)$, it gives more weight to short times than using a constant time lag and provides a better fit to the first part of the curve.

4.2.3. GPS Data for Nias

[67] We used the postseismic displacement estimated from GPS data by *Hsu et al.* [2006]. The displacement was resampled using a logarithmic time scale. Three sites were installed 5 months after the main shock, and were not considered in this study. The measurements at the seven other sites are available from 0.5 to 331 days after the main shock. The cumulated afterslip (horizontal displacement) ranges from 5 to 60 cm.

4.2.4. GPS Data for Denali

[68] We used the GPS data analyzed by *Freed et al.* [2006a, 2006b]. A few sites were installed before the main shock, and other a few weeks after. *Freed et al.* [2006a, 2006b] studied postseismic deformation of Denali earthquake both from an inversion of GPS displacements and from stress-driven forward models, poroelastic rebound, viscoelastic flow and afterslip. They concluded that no single mechanism can explain the postseismic observations but that a combination of several mechanisms is required. Afterslip within the upper crust occurs adjacent to and beneath the regions of largest coseismic slip. There is likely deeper afterslip, in the middle and lower crust, but afterslip cannot be distinguished from broad viscoelastic flow. We used the 16 sites that were installed less than 22 days after the main shock, and analyzed the measurements until 1436 days after the main shock. The cumulated afterslip at these sites during the first 1436 days ranges between 3 and 26 cm. The observations were corrected for offset and periodic terms [*Freed et al.*, 2006a]. We used the original daily solutions without resampling.

4.3. Fit of Afterslip Data

4.3.1. Fit by Omori Law

[69] The Omori law, initially suggested to fit aftershock rate, has also frequently been used to fit afterslip rate [*Wennerberg and Sharp*, 1997; *Montési*, 2004; *Langbein et al.*, 2006]. The expression for the postseismic displacement is

$$\delta = \frac{V_0 t^* \left[(1 + t/t^*)^{1-p} - 1 \right]}{1 - p} + V_l t, \tag{49}$$

where V_l is a constant loading rate, that may be either positive or negative (afterslip with direction opposite to interseismic deformation). This law was also derived assuming a power law rheology in the region where afterslip occurs [*Montési*, 2004]. Such a rheology is appropriate if that region is a greater depth than the seismogenic zone, so ductile creep is activated. We have thus four parameters to estimate. The inversion was performed using a Nelder-Mead algorithm, with 50 different sets of initial values.

4.3.2. Fit by the Rate-Dependent Friction Law

[70] We used the friction law proposed by *Perfettini and Avouac* [2004] and *Montési* [2004] to describe afterslip of velocity-strengthening fault patches. *Hsu et al.* [2006] used a slightly more complex form of the slip rate than expres-

Table 3. Results for Parkfield GPS and Creepmeter Data[a]

Site	δ_{max}	Omori Law					Velocity-Strengthening Friction					R&S Friction	
		V_0	t^*	p	V_l	rms	V_1	V_2	t_a	V_0/V_l	rms	B/A	rms
CAND	101.	11798.	0.00002	0.70	−0.0177	1.78	0.080	0.003	4064.	4331.	2.13	0.97	**1.75**
HOGS	46.	13.4	1.01685	1.28	0.0172	1.88	−0.218	0.254	32.	65.	1.90	0.33	**1.87**
HUNT	115.	22228.	0.00004	0.79	0.0151	1.59	0.144	0.031	270.	4131.	2.06	3.64	**1.51**
LAND	70.	38.0	0.26716	1.02	0.0008	1.46	−0.049	0.074	127.	543.	1.46	0.74	**1.43**
MASW	46.	13.3	0.86885	1.20	0.0102	1.62	−0.121	0.148	51.	108.	1.63	0.12	**1.59**
MIDA	132.	4.4e5	0.00000	0.76	−0.0187	2.85	0.127	0.008	1519.	5669.	3.40	0.96	**2.81**
MNMC	80.	640.0	0.00015	0.60	−0.0457	1.80	0.052	0.001	7782.	2852.	1.87	0.83	**1.78**
RNCH	48.	16.8	0.55945	1.22	0.0324	2.33	−0.172	0.223	27.	89.	2.33	1.04	**2.33**
TBLP	77.	9767.	0.00003	0.74	0.0256	2.09	0.077	0.010	757.	1028.	2.32	12.2	**2.04**
POMM	72.	16.3	0.97518	1.16	0.0136	1.72	−0.188	0.233	50.	80.	1.723	0.66	**1.72**
crr1	129.	82.8	0.03489	0.66	−0.1548	0.74	0.054	0.002	1.1e4	9979.	1.24	0.91	**0.68**
tabc	149.	3400.	0.00005	0.59	−0.3326	1.18	0.032	0.000	9.6e4	52749.	2.86	0.92	**0.72**
wkr1	128.	3.1	55.0674	2.45	0.1058	0.43	−1.295	1.439	58.	3.2	0.39	0.61	**0.28**
xgh1	66.	113.2	0.04534	0.89	−0.0125	0.70	0.037	0.002	4688.	36415.	0.81	5.60	**0.53**
xmbc	179.	122.1	0.14702	0.97	0.1532	1.53	0.174	0.003	6435.	35625.	1.55	0.57	**1.19**
xmd1	133.	63.0	0.31867	0.94	−0.1544	0.77	−0.127	0.010	2477.	5106.	0.79	1.23	**0.62**
xmm1	194.	85.3	0.37962	1.13	0.2449	1.15	0.045	0.220	96.	609.	1.32	0.58	**0.65**
xta1	159.	32.7	0.29500	0.73	−0.1230	0.65	0.035	0.026	1114.	664.	0.93	0.84	**0.42**
xva1	169.	128.9	0.20825	1.06	0.0602	1.45	0.024	0.011	1977.	15737.	1.52	0.45	**0.72**

[a]Parkfield data are the first 10 lines. Times are in days and displacements in mm. Bold font indicates the best fit.

sion (23) to fit afterslip data for Nias. They introduced geometrical factors to account for the variation of displacement with distance from the fault. The expression for the displacement is thus given by

$$\delta = V_1 t + V_2 t_a \log\left[1 + \frac{V_0}{V_l}\left(e^{t/t_a} - 1\right)\right], \quad (50)$$

where V_1 and V_2 are proportional to the loading rate. We have fitted the displacement to invert for V_1, V_2, t_a and V_0/V_l, using a broad range of initial values.

4.3.3. Fit by the Rate-and-State Friction Law

[71] We solve numerically for the rate-and-state friction law (1 and 2) with a constant loading rate. There are seven parameters in the model: the initial slip rate V_0 and friction μ_0, the critical slip distance D_c, the normalized stiffness k/k_b, the friction parameters A, B, and the loading rate V_l. We have run the optimization starting with more than 100 different initial values for each data set, with a broad range of values (lognormal distribution of A, D_c, k/k_b, V_0, V_l, and gaussian distribution of B/A and $(\mu_0 - \mu_{ss})/B$). Although the surface displacement measured by GPS at some distance from the fault is smaller than the afterslip on the fault, we did not account for the decrease in amplitude with the distance from the fault. While afterslip is larger than displacement at some distance from the fault, both variables have the same evolution with time. By neglecting attenua-

tion with distance, we have underestimated afterslip, likely by underestimating D_c or V_0. We could have introduced a constant factor in the model to correct for this effect, as done by *Perfettini and Avouac* [2004] or *Hsu et al.* [2006], but the number of parameters in the full rate-and-state model is already very large so that the parameters are not constrained.

4.4. Results

[72] The results for each data set are listed in Tables 3–5, and the best fits are shown in Figures 6–9. In many cases all models produce very similar fits, so curves are superposed in Figures 6–9. Figure 10 shows a map of residuals for GPS station CAND at Parkfield. The residuals are plotted as a function of p and t^* for Omori law, V_0/V_l and t_r for the rate-dependent friction law, and B/A and k/k_b for the rate-and-state friction law, with other parameters fixed to the best fit value. The size of the gray area in these plots, corresponding to residuals smaller than twice the min value, give an idea of the uncertainty on the model parameters, and highlight the correlation between some parameters.

4.4.1. Omori Law

[73] Usually, the Omori exponent p is close to 1 and t^* is of the order of hours or days. But, at least for a few cases, p-value is significantly different from 1 (see Figure 10a). For a few sites, the inversion yields very small t^* value, which could not be distinguished from zero (see Figure 10a). In

Table 4. Results for Nias[a]

Site	δ_{max}	Omori Law					Velocity-Strengthening Friction					R&S Friction	
		V_0	t^*	p	V_l	rms	V_1	V_2	t_a	V_0/V_l	rms	B/A	rms
BSIM	235.	520.6	0.0114	0.72	−0.2003	1.62	−0.007	0.022	2297.	707.	1.95	1.21	**1.55**
LEWK	110.	0.9	408.8	5.12	0.0914	1.51	−66.76	66.89	83.	1.01	1.59	1.63	**1.44**
LHWA	606.	3703.	0.0039	0.76	−0.3335	**2.20**	0.027	0.005	25948.	8354.	3.51	0.69	2.29
PBAI	52.	15.9	0.2414	0.63	−0.2528	**1.41**	−0.119	0.002	8889.	2221.	1.45	3.59	1.43
PSMK	244.	19.9	2.5427	0.97	−0.0416	1.65	−0.039	0.022	2528.	864.	1.65	1.84	**1.63**
PTLO	151.	11.4	4.3866	1.06	−0.1206	1.49	−0.385	0.363	132.	30.	**1.45**	5.57	1.46
SAMP	52.	3.2e5	0.0000	0.80	−0.1014	1.35	−0.061	0.007	1869.	1567.	1.35	1.55	**1.34**

[a]Bold font indicates the best fit.

Table 5. Results for Denali[a]

Site	δ_{max}	Omori Law					Velocity-Strengthening Friction					R&S Friction	
		V_0	t^*	p	V_l	rms	V_1	V_2	t_a	V_0/V_l	rms	B/A	rms
299C	38.	7.02	7.0e4	0.25	−6.977	1.87	−6.129	2.0650	4.8e5	3.0	1.87	2.91	**1.80**
CLGO	41.	24.77	0.048	0.83	0.007	1.78	0.008	0.0017	2480.	1099.4	1.79	8.88	**1.69**
DRMC	261.	1.45	47.8	1.19	0.072	1.88	−0.018	0.1074	511.	14.5	1.87	0.18	**1.85**
GRNR	19.	0.01	3.8e9	1.2e7	0.0003	2.20	−0.004	0.0040	501.	2.9	2.20	1.03	**2.16**
LOGC	123.	0.15	1.3e4	20.0	0.010	3.15	−0.142	0.1413	1214.	2.2	3.16	1.49	**3.10**
FAIR	39.	0.58	0.506	0.41	−0.013	1.79	0.003	0.0009	9949.	129.2	1.80	2.74	**1.76**
HIWC	47.	0.91	0.030	0.27	−0.034	1.96	0.004	0.0003	54930.	309.3	1.97	1.01	**1.92**
MENT	222.	0.75	344.5	3.29	0.088	1.97	−0.199	0.2910	259.	4.2	**1.97**	0.49	1.98
FRIG	203.	1.26	29.5	0.97	0.046	1.99	0.048	0.0002	1.87e5	5810.1	1.99	1.38	**1.98**
HURC	56.	0.12	1.8e6	1.1e4	0.025	2.12	−0.099	0.1239	216.	2.3	2.12	1.55	**2.10**
PAXC	204.	1.57	25.9	1.11	0.066	1.82	0.029	0.0487	686.	36.9	1.82	4.32	**1.1**
CENA	27.	4.82	1.2e5	0.48	−4.788	2.09	−15.20	1.2704	8.4e6	12.0	2.09	12.2	**1.96**
DNLC	107.	4.91	0.229	0.49	−0.052	**1.90**	−0.010	0.0005	86495.	849.6	1.91	1.76	1.90
GNAA	104.	0.15	5.1e9	3.2e7	0.055	1.89	−0.028	0.0814	264.	3.4	1.91	0.85	**1.82**
JANL	92.	1.80	0.265	0.38	−0.048	1.94	0.001	0.0024	14787.	97.7	2.00	2.94	**1.78**
TLKA	55.	0.66	2.510	0.04	−0.491	2.52	−0.004	0.0008	42618.	128.5	2.53	1.38	**2.47**

[a]Bold font indicates the best fit.

other cases, especially for Denali, the inversion produced very large values of both t^* and p. In that case Omori's law is very close to an exponential relaxation with a characteristic time equal to t^*/p. We found both positive and negative values for the loading rate V_l. But in most cases, V_l is not constrained and cannot be distinguished from zero. Omori law generally fitted the data almost as well as the rate-and-state model, and even better in two cases, but with only four parameters compared to seven for rate-and-state friction.

4.4.2. Rate-Dependent Friction

[74] In many cases the parameters were not well constrained. The inversion often converged to very large values of t_a and V_0/V_l. In this regime, the rate-dependent friction law is equivalent to a logarithmic increase of slip with time (i.e., an Omori law with $p = 1$ for slip rate) as predicted by expression (39). Afterslip duration is highly variable from one site to another one. For Parkfield, its median value is 3 years, 17 years for Denali, and 6.3 years for Nias. A few inversions yielded very large values of V_1 and V_2 of opposite sign, up to several cm/day. Such values are clearly unphysical, because both V_1 and V_2 should be smaller than tectonic loading rate. The ratio V_0/V_l has a median value of 576. It is larger for Parkfield than for the two other events. This law has the same number of parameters as Omori's law, but most of the time was not as good in fitting the data. Omori law provided a better fit than the rate-dependent friction law in 34 out of 42 cases.

4.4.3. Rate-and-State

[75] Because the simple Omori law with four parameters already provides a good fit to the data, it seems unrealistic to invert reliably for the seven parameters of the rate-and-state law. Indeed, we find that there is a huge range of model parameters that fit the data within the measurement resolution. The inverted parameters appear to be mostly constrained by our choice of initial values in the optimization. The map of residuals in Figure 10c for station CAND is very focused around the best fit value of B/A, but k/k_b can't be distinguished from zero, and there are many other local minima with very different parameters but similar residuals.

[76] The distribution of final models which gave a good fit to the data was very similar to the distribution of initial values used for the optimization. The only difference was for the critical slip distance. While the initial critical slip distance had a typical value of 0.1 mm, most best fits had D_c larger than 1 mm. D_c was found to range between 0.05 and 860 mm, with an average of 42 mm and a median of 4 mm. The critical slip distance for the best fit is increasing (with huge fluctuations) with the cumulative postseismic displacement. The ratio D_c/d_{max} in Tables 3−5 is on average 0.23, with a median value of 0.056. Critical slip distance is thus generally much lower than total afterslip. The median value of D_c increases with the main shock magnitude; it is equal to 1.8 mm for Parkfield, 5.2 mm for Denali and 21 mm for Nias earthquake.

[77] For most data sets we cannot distinguish between the velocity-weakening and velocity-strengthening regimes, both cases could fit the data as well (see Figures 6−9). Velocity-weakening models better fitted the data than velocity-strengthening parameters in 24/42 cases. Although this model has the largest number of adjustable parameters, it gave the best fit only for 37 sites out of 42. There is no correlation between the Omori exponent p and the ratio B/A for the best fit, while the analytical study predicted that $p = B/A$ for stress much lower than steady state friction.

[78] The stiffness was found to be of the order of k_B, but this was also true for the choice of initial parameters. This ratio was found to be smaller for velocity-strengthening models than for velocity weakening. The stiffness for best fits is always larger than the threshold k_c for instabilities. But for a few sites we also found models with $k < k_c$ that produced a similar quality of fit. GPS measurements are more sensitive to shallow afterslip than deeper slip, and creepmeters directly measure surface slip. Shallow fault patches have smaller normal stress, hence smaller k_c and larger k/k_c. So the ratio k/k_c should be smaller at greater depth, where earthquakes nucleate.

5. Seismicity Rate Triggered by Afterslip

5.1. Relation Between Stress and Seismicity

[79] Previous studies [*Rice and Gu*, 1983; *Dieterich*, 1994; *Schaff et al.*, 1998; *Perfettini and Avouac*, 2004; *Hsu et al.*, 2006; *Bourouis and Bernard*, 2007; *Savage et al.*, 2007] have already suggested that afterslip can trigger
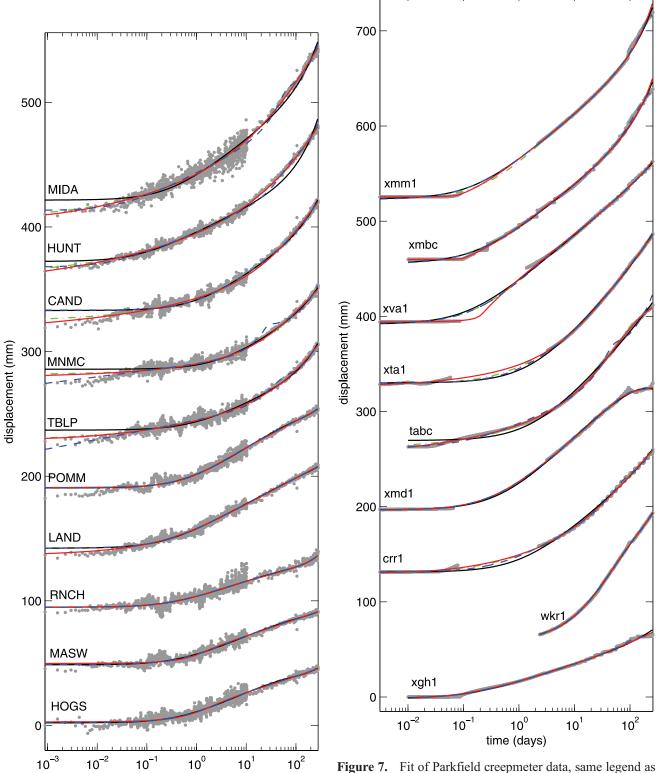
Figure 6. Fit of Parkfield GPS data (grey dots, with arbitrary offset) by Omori's law (dashed-dotted green curve) by the rate-dependent friction law (solid black curve) and by the rate-and-state law (solid red curve is best fit with $A > B$, dashed blue curve is best fit with $A < B$).

Figure 7. Fit of Parkfield creepmeter data, same legend as in Figure 6.

aftershocks by reloading parts of the fault that are locked after the main shock. The fact that aseismic slip can trigger seismicity has also been demonstrated for swarms induced by slow earthquakes at Hawaii [*Segall et al.*, 2006] and in the Salton Trough [*Lohman and McGuire*, 2007]. Most studies who suggested that aftershocks are due to afterslip
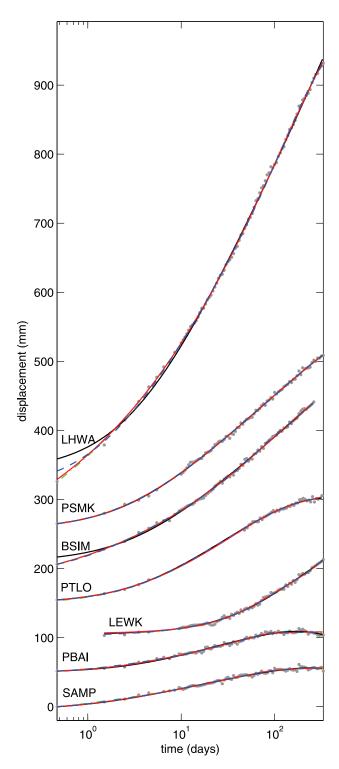
Figure 8. Fit of Nias GPS data, same legend as in Figure 6.

assumed that aftershock rate is simply proportional to stress or strain rate [*Wennerberg and Sharp*, 1997; *Schaff et al.*, 1998; *Perfettini and Avouac*, 2004; *Hsu et al.*, 2006; *Savage et al.*, 2007]. However, *Dieterich* [1994] showed that the relation between seismicity rate and stress rate can be much more complex. For instance, in the case of a simple stress step $\Delta\tau$ followed by a constant stressing rate $\dot{\tau}_l$, the

seismicity rate $R(t)$ is given by *Dieterich* [1994]

$$R(t) = \frac{r}{(e^{-\Delta\tau/A\sigma} - 1)e^{-t/t_a} + 1}, \tag{51}$$

r is the seismicity rate for a constant stressing rate equal to $\dot{\tau}_l$. Aftershock rate increases immediately after the stress step. At intermediate times, for $\exp(-\Delta\tau/A\sigma) \ll t/t_a \ll 1$, aftershock rate decreases according to Omori law $R(t) \approx rt_a/t$. Seismicity rate recovers the background rate r for times much larger than the nucleation time t_a. Typically, t_a is of the order of years [*Dieterich*, 1994]. This shows that there can be a very long time delay between a change in stress and triggered seismicity. The assumption that aftershock rate is proportional to stress rate for earthquakes triggered by afterslip thus needs to be verified.

[80] *Dieterich* [1994] derived a general relation between stress rate and seismicity rate, which can be used to model seismicity triggered by afterslip

$$R = \frac{r}{\gamma\dot{\tau}_l}, \tag{52}$$

where γ is a seismicity state variable, which evolves as

$$\dot{\gamma} = \frac{1}{A\sigma}(1 - \gamma\dot{\tau}). \tag{53}$$

Dieterich [1994] used this model to estimate the seismicity rate for different loadings, such as a coseismic stress change, a constant stressing rate, or a logarithmic increase or decrease of stress with time. He showed that both a coseismic stress step, or a logarithmic stressing can produce an Omori law decay of aftershocks with time. The Omori exponent is equal to 1 for a stress step but may be either smaller or larger than 1 in the case of a logarithmic loading (see Figure 8 and equation (B21) of *Dieterich* [1994]).

[81] We can rewrite (53) as

$$\frac{-A\sigma\dot{\gamma} + 1}{\gamma} = \dot{\tau}. \tag{54}$$

Integrating (54) and using the definition (52), we get a simple form for the relation between seismicity rate R, cumulative number of events $N = \int_0^t R\,dt$, and stress change $\tau = \int_0^t \dot{\tau}\,dt$

$$A\sigma \ln\left(\frac{R}{R_0}\right) + \frac{N\dot{\tau}_l}{r} = \tau. \tag{55}$$

[82] For R changing slowly in time, we can neglect the first term in (55). So the seismicity rate is proportional to the stressing rate, specifically

$$R = \frac{r\dot{\tau}}{\dot{\tau}_l}. \tag{56}$$

This approximation is valid as long as $\ln(R/R_0) \ll N/rt_a$, which is equivalent to $r\dot{R}/R^2 \ll 1/t_a$. In the case of periodic fluctuations, this approximation is valid if the period is much longer than t_a.
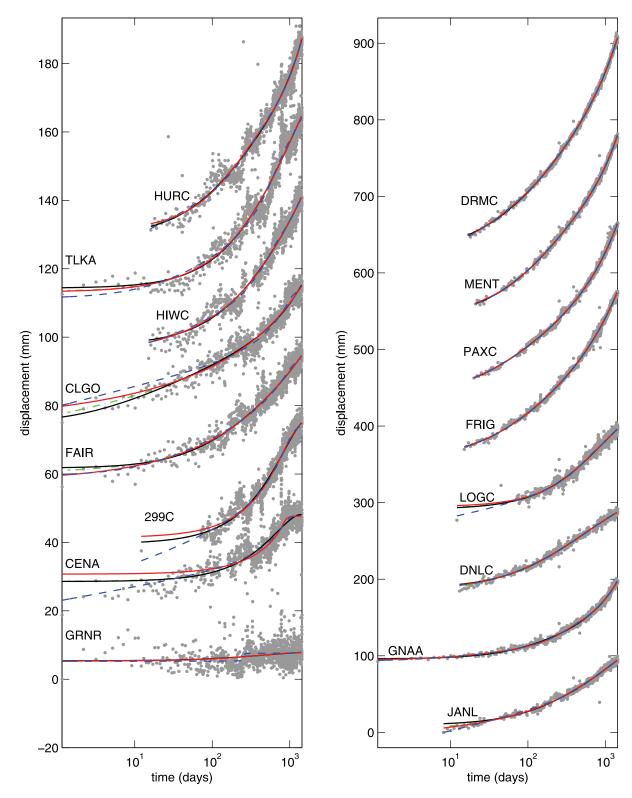
Figure 9. Fit of Denali GPS data, same legend as in Figure 6.

[83] For rapid variations of seismicity rate, we can neglect the second term in (55). The seismicity rate thus increases exponentially with stress

$$R = R_0 e^{\tau/A\sigma}. \tag{57}$$

Beeler and Lockner [2003] measured the correlation between seismicity rate and stress in laboratory friction experiments, with a periodic perturbation of the stress rate superposed to a constant loading rate. They found that the relation between seismicity rate and stress is in good
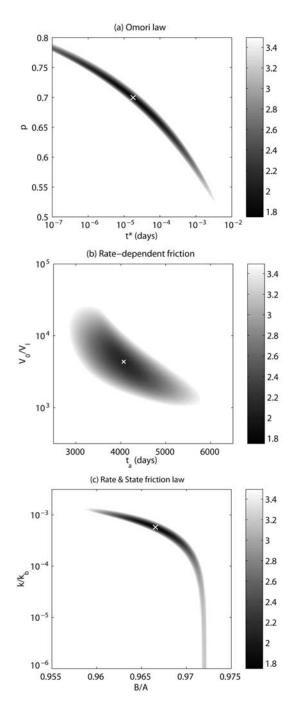
Figure 10. Map of residuals (in mm) for GPS station CAND at Parkfield. (a) Residuals for Omori law as a function of p and t^*; (b) residuals for the rate friction law as a function of V_0/V_l and t_r; (c) residuals for the rate-state friction law as a function of B/A and k/k_b. All other model parameters are fixed to the best fit value. The white cross in each plot shows the best fit parameters.

agreement with expression (56) for slow stress changes, and with equation (57) for fast stress changes. Expression (57) also provides a good fit to seismicity triggered by tides [*Cochran et al.*, 2004], though the small values of the stress change $\tau/A\sigma$ do not allow to test if R increases proportionally or exponentially with τ.

5.2. Application to Model Seismicity Triggered by Afterslip

5.2.1. Stress Rate

[84] Initial stress on the fault is likely to be very heterogeneous, owing to variations of coseismic slip. As a consequence, areas of the fault that are approximately locked after the main shock will be reloaded by adjacent areas with larger slip rate. We model the stress rate induced by afterslip as

$$\dot{\tau} = \frac{\dot{\tau}_0}{(1 + t/t^*)^p}. \tag{58}$$

Following *Dieterich* [1994], we consider both the influence of a postseismic loading ($\dot{\tau} > 0$) or relaxation ($\dot{\tau} < 0$) on a population of active faults.

5.2.2. Special Case $p = 1$

[85] There is an analytical solution for the seismicity rate with stress following (58) only for the special case $p = 1$ (equation (B21) of *Dieterich* [1994])

$$R = \left[\frac{(1 + t/t^*)^{-m}}{R_0} + \frac{(1 + t/t^*) - (1 + t/t^*)^{-m}}{r(m+1)t_a/t^*} \right]^{-1}, \tag{59}$$

where m is defined by

$$m = \dot{\tau}_0 t^*/A\sigma, \tag{60}$$

and can be either positive (reloading) or negative.

[86] In the case of a positive stressing rate ($m > 0$), the seismicity rate first increases with time and reaches its maxima for time equal to

$$t_m = t^* \left[\left(\frac{m(m+1)rt_a}{R_0 t^*} - m \right)^{1/(m+1)} - 1 \right]. \tag{61}$$

As postseismic stress change increases, t_m decreases.

[87] Including a coseismic stress step $\Delta\tau$ is equivalent to increasing initial rate $R_0 = r \exp(\Delta\tau/A\sigma)$, if seismicity rate is equal to the background rate at the time of the main shock. Increasing the coseismic stress change also decreases the peak time t_m. For very large coseismic stress change, t_m given by (61) becomes negative. In this case, seismicity rate decreases continuously toward the background rate. In all cases, the long-time behavior of seismicity rate for $t \gg t_m$ is only controlled by afterslip, while the short-time rate is controlled by coseismic stress.

[88] For times larger than t_m, seismicity rate predicted by (59) for $m > 0$ decreases proportionally to the stress rate

$$R \approx \left(1 + \frac{1}{m} \right) \frac{r\dot{\tau}}{\dot{\tau}_l}. \tag{62}$$
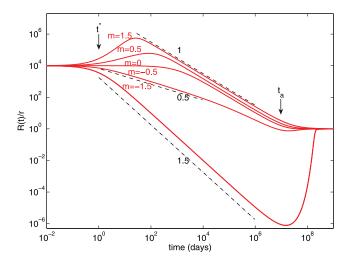
Figure 11. Seismicity rate triggered by a continuous stress change given by $\dot{\tau} = \dot{\tau}_0/(1 + t/t^*) + \dot{\tau}_l$ with $A\sigma = 0.1$ MPa, $t^* = 1$ day, $\dot{\tau}_l = 10^{-5}$ MPa/day and for different amplitudes of the postseismic stress change $m = \dot{\tau}_0 t^*/A\sigma$, from $m = -1.5$ (bottom) to $m = 1.5$ (top). In addition to the postseismic loading, we assume a coseismic stress increase of amplitude $\Delta\tau = a\ln(R_0) = 0.92$ MPa so that the initial seismicity rate $R_0 = r \times 10^4$ is much higher than the background rate. The case $m = 0$ represents seismicity rate triggered only by the coseismic stress step.

[89] For a postseismic unloading, m is negative and the first term in (59) dominates at early times so that $R \approx R_0 (1 + t/t^*)^m$ [*Dieterich*, 1994]. This model can thus explain observations of aftershock decay with Omori exponents that are either smaller or larger than one. Seismicity rate decreases below the background rate, and increases back to r for $t > t_a$. Relaxation due to afterslip may thus also explain observations of delayed quiescence. However, this requires that the zone is first subject to coseismic stress loading, to increase seismicity rate well above the background rate. At the same time, the area must be unloaded by adjacent slipping faults. If afterslip mostly occurs below the fault at depth, then postseismic stress unloading requires either target fault planes oriented at very different angle from the main fault, or relatively remote target faults. So this mechanism for explaining delayed quiescence might not be a common one.

[90] Typical examples of aftershocks rate are shown in Figure 11 both for postseismic reloading ($m > 0$) or unloading ($m < 0$). We have superposed a coseismic step, a postseismic stress change and a constant background rate in order to compare the relative influence of coseismic and postseismic stress changes on seismicity rate.

5.2.3. General Case $p \neq 1$

[91] Changing the exponent p of the temporal decay of afterslip also affect the Omori exponent of triggered seismicity. Typical evolutions of seismicity rate are shown in Figure 12 for $p = 1.3$ and $p = 0.8$. For $p \neq 1$ and $m > 0$, we found numerically that expression (61) is still a rather good approximation of the time t_m at which R reaches its maximum (see Figure 12). At intermediate times $t_m < t < t_a$, expression (62) also provides a good fit to the seismicity rate; that is, the seismicity rate is proportional to stress rate. However, if $p > 1$, we found in numerical simulations of

(55) that there is a time t_c after which expression (62) does not hold.

[92] If $p > 1$, stress and thus number of events N saturate for $t \gg t^*$. The stress change increases toward a maximum value τ_{max} given by

$$\tau_{max} = \int_0^\infty \dot{\tau} dt = \frac{\dot{\tau}_0 t^*}{p - 1}. \tag{63}$$

The first term $\sim \ln(R)$ becomes non negligible compared with the term $\sim N$ in the stress-seismicity relation (55). The seismicity rate for large times $t > t_c$ is equivalent to that triggered by an instantaneous stress step of amplitude $\Delta\tau$, described by equation (51). The transition from the regime $R \approx r\dot{\tau}/\dot{\tau}_l$ (62) for $t_m \ll t \ll t_c$ to the regime $R \approx rt_a/t$ for $t \gg t_c$ occurs at a time t_c given by $\dot{\tau}(t_c) = A\sigma/t_c$. Assuming $t_c \gg t^*$, we get

$$t_c \approx t^* m^{1/(p-1)}. \tag{64}$$

[93] If there is a nonzero constant stress rate $\dot{\tau}_l$, in addition to the stress rate (58) induced by afterslip, seismicity rate decays as the inverse of time for $t_c \ll t \ll t_a$, until it reaches its background level r. The number of events triggered by afterslip can be computed directly from (55). When R returns to its background rate and stress has reached its limit value τ_{max}, the first term is equal to zero in (55) and $N = r\tau_{max}/\dot{\tau}_l$. This result is independent of the form of the stress change, as long as stress reaches a maximum value τ_{max} at long times. The stress change needed to explain the observed number of aftershocks is thus the same for static triggering and for triggering due to afterslip.

[94] For a slow decay of stress rate with time ($p < 1$), stress does not saturate for $t \gg t^*$ but instead increases as $\tau = \int_0^t \dot{\tau} dt \sim t^{1-p}$ for $t \gg t^*$. Seismicity rate thus never reaches the
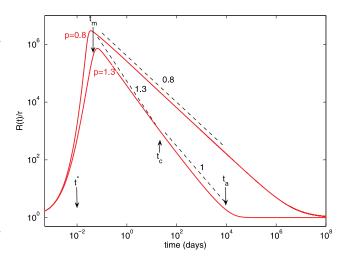

Figure 12. Seismicity rate triggered by a continuous stress change given by $\dot{\tau} = \dot{\tau}_0/(1 + t/t^*)^p$ with $p = 0.8$ (top) or $p = 1.3$ (bottom), $R_0 = r$, and $m = 10$. For $p = 1.3$, the crossover time t_c given by (64) is 21.5 days and marks the transition between a $\sim 1/t^p$ decay of seismicity rate for $t_m < t < t_c$ to the long time $\sim 1/t$ decay. For $p = 0.8$, seismicity rate is proportional to stressing rate after the end of the accelerating phase for $t > t_m$.

regime described by (51) with $R \sim 1/t$. In this case, seismicity rate is proportional to stress rate as predicted by (62) for $t > t_m$.

[95] This work shows that seismicity rate triggered by afterslip does not always scale with slip rate, as generally assumed. For instance, we can observe $V \sim \dot{\tau} \sim t^{-p}$ with $p > 1$ but $R \sim 1/t$. The characteristic times t_m and t_c that control seismicity rate are also different from the characteristic time t^* which controls afterslip rate. The Omori exponent may be either smaller or larger than 1, and is controlled both by the exponent p of the temporal evolution of stressing rate and by its amplitude m (if $m < 0$).

5.2.4. Comparison With Aftershock Data

[96] Aftershock studies [*Helmstetter et al.*, 2005; *Peng et al.*, 2007] have shown that seismicity rate decreases with time according to $R \sim R_0/(1 + t/c)^{\rho}$, with a characteristic time c that is no larger than 10 s, and an exponent ρ that can be either smaller or larger than 1, and is usually between 0.9 and 1.2 [*Reasenberg and Jones*, 1994; *Helmstetter et al.*, 2003]. At very short times, the aftershock decay may be slower. *Peng et al.* [2007] found an exponent of ≈ 0.6 for times shorter than 900 s, when stacking aftershock sequences of shallow main shocks in Japan. Seismicity rate can increase by a factor up to 10^5 relative to the background rate. The duration of aftershock sequences is of the order of years, i.e., about 10^6 larger than the characteristic time c.

[97] In order to explain aftershock triggering by afterslip, we need the characteristic times t^* to be of the order of seconds. This is much smaller than the values of t^* of a few days estimated for afterslip data following Superstition Hills earthquake [*Wennerberg and Sharp*, 1997], or for Nias, Parkfield and Denali earthquakes (see Tables 3–5). However, afterslip was measured at the surface, we can expect strong fluctuations of t^* with depth owing to changes of friction parameters or initial values. t^* may thus be much smaller at depth, where aftershocks nucleate. It is also badly constrained from afterslip data. Tables 3–5 shows that for many data sets we cannot exclude the value $t^* = 0$.

[98] The characteristic time c of aftershock rate is also difficult to estimate from seismicity catalogs, because seismic networks are always saturated after a large event. The detection threshold is much larger than usual for a period that can last for more than a week depending on the minimum magnitude considered, on the seismic network and on the main shock magnitude [*Kagan*, 2004; *Helmstetter et al.*, 2005]. For Nias earthquake, *Hsu et al.* [2006] found that both displacement and aftershock number increase logarithmically with time $\sim \ln(1 + t/t^*)$, with $t^* \approx 3$ days. However, they counted the number of $m > 3$ aftershocks triggered by the main shock, while the catalog is not complete for such small events, and the completeness level decreases with time after the main shock. Using only $m \geq 5.5$ aftershocks, we measured $c \approx 0.1$ day, much smaller than the characteristic time t^* of afterslip inferred from GPS measurements. But when fitting Omori's law to the displacement time series, we found that, for three out of eight points, the short-time cutoff c is much smaller than 1 day, and cannot be distinguished from zero (see Table 4).

[99] As shown above, the stress change involved to trigger N events is the same for static triggering and for triggering by afterslip. Because the amplitude of afterslip is often comparable to coseismic slip [*Takai et al.*, 1999; *Melbourne et al.*, 2002; *Pritchard and Simons*, 2006] or

even larger [*Heki et al.*, 1997; *Langbein et al.*, 2006], the number of events triggered by afterslip should be comparable to that triggered by coseismic stress change. If $p \approx 1$, or for static triggering, the stress change needed to produce an increase of seismicity rate by a factor 10^5 is equal to $A\sigma \ln(10^5) = 11.5A\sigma$. If $A\sigma \approx 0.1$ MPa, as suggested by *Cochran et al.* [2004], this gives realistic values, smaller than the average stress drop. On the other hand, if we use the laboratory value $A \approx 0.01$ [*Dieterich*, 1994], and a normal stress $\sigma = 100$ MPa (of the order of the lithostatic pressure at a depth of about 5 km), then the stress change needed is 11.5 MPa. This seems quite large, however it is possible that maximum stress change can locally reach such values. As shown by *Helmstetter and Shaw* [2006], seismicity rate triggered by a heterogeneous stress change at short times is controlled by the maximum stress change rather than the mean value.

[100] *Perfettini and Avouac* [2007] argue that reloading due to afterslip is the sole mechanism for aftershock triggering, because triggering by static stress change is assumed to be immediate, and thus cannot be distinguished from the main shock rupture. This would be true only if the characteristic duration of aftershock sequences t_a was of the order of seconds within the seismogenic zone, but of the orders of years in the main afterslip zone above and below the seismogenic zone. Such a huge variation of t_a with depth is difficult to explain. Is it however likely that many events triggered by the coseismic stress change occur at very short times after the main shock and are not detected [*Kagan*, 2004; *Peng et al.*, 2007]. In contrast, postseismic stress change is more progressive, thus aftershocks triggered by afterslip won't be mixed up with the main shock. Therefore, afterslip may be more efficient for triggering than static changes for the same seismic moment.

[101] In our model, Omori exponent is controlled both by the temporal decay of afterslip and by its amplitude. One solution to explain Omori exponents larger than 1 it to assume that afterslip also decays faster than $1/t$. For instance, following the 1992 M_w7.3 Landers earthquake, the seismicity rate decreased with time as $R \sim t^{-1.2}$ over 5 decades in time. We found numerically that in order to reproduce this pattern with $p = 1.2$ and $R_0 = r$ (no coseismic stress change), we need a stress change τ_{max} of about 50 $A\sigma$. Another explanation for this fast aftershock decay is to assume a superposition of coseismic stress increase and postseismic unloading. To produce an instantaneous increase of R by a factor 10^6, we need a (maximum) stress step of about $14A\sigma$. The following $1/t^{1.2}$ aftershock decay can be explained by a postseismic relaxation with $m = -1.2$ and $p = 1$. The corresponding stress released by afterslip up to a time $\approx 10^5 t^*$ is $A\sigma m \ln(10^5) \approx 14A\sigma$. Thus, the combination of coseismic loading and postseismic unloading, with $p = 1$ and $m = -1.2$, requires a smaller stress change than reloading by afterslip.

6. Conclusion

[102] We have modeled postseismic slip using the rate-and-state friction law. The postseismic behavior of faults is more complex than predicted previously on the basis of steady state approximation of the friction law. We found that, depending on the model parameters B/A and k, and on

initial friction, the fault exhibits either decaying afterslip, slow earthquakes, or aftershocks. Afterslip, with slip amplitude comparable or even larger than D_c, can be obtained for any value of the friction law parameters, even for velocity-weakening faults ($A < B$).

[103] We have shown that the complete rate-and-state law provides a good fit to afterslip data for Nias, Parkfield, and Denali earthquake. This law provides a slightly better fit than the frequently used rate-dependent friction law. But the number of parameters of the rate-and-state model is too large to reliably estimate the model parameters. For most data sets we studied, afterslip can be modeled as well with velocity-weakening or velocity-strengthening friction parameters, and the fit by the full rate-and-state law is not much better than the fit by Omori's law or by the rate-dependent friction law.

[104] Most studies assume that frozen heterogeneities in friction properties (A/B or D_c) control the behavior of the Earth crust and the transition between aseismic and seismic slip [*Boatwright and Cocco*, 1996; *Miyazaki et al.*, 2004; *Hsu et al.*, 2006; *Johnson et al.*, 2006; *Perfettini and Avouac*, 2007; *Bourouis and Bernard*, 2007]. Small earthquakes located within otherwise creeping faults are explained as velocity-weakening asperities embedded in a velocity-strengthening fault [*Boatwright and Cocco*, 1996; *Bourouis and Bernard*, 2007]. Multiplet relocations on creeping segments have shown that multiplets occur over and over at the very same place, so that there exists some strong structural control on the local seismic regime. While variations of A and B with depth are expected from laboratory friction experiments and likely explain large-scale variations of frictional behavior with depth, small-scale lateral variations are more difficult to explain, but might result from variations in pore pressure, normal stress or the properties of the fault material [*Boatwright and Cocco*, 1996]. We have shown here that stress heterogeneity can also control frictional behavior and introduce complexity in faults dynamics [*Hirose and Hirahara*, 2004]. Stress heterogeneity may be either frozen (e.g., due to fault geometry) or evolving with time after each main shock. Thus, slow earthquakes or afterslip may be associated with velocity-weakening faults, which are also able to produce slip instabilities if stress becomes large enough.

[105] Aftershock decay with time (Omori law) is similar to that observed for afterslip rate. This similarity led several authors to suggest that aftershocks are induced by the postseismic reloading of the fault due to afterslip. Using the relation between stress and seismicity derived by *Dieterich* [1994], we have shown that afterslip is indeed a possible mechanism to explain aftershock triggering. But the relation between slip rate and seismicity rate is more complex than previously thought. The process of earthquake nucleation indeed introduces a time delay between stress change and triggered earthquakes. As a consequence, seismicity rate is characterized by exponents and characteristic times that can be different from those that control stress rate. The complexity of the friction law thus makes it difficult to infer the mechanisms responsible for earthquake triggering on the basis of observations of stress changes. Moreover, we have simplified the problem by considering uniform values of the model parameters, and of the slip rate, by modeling the fault with a simple slider block with one degree of freedom. We

have also neglected other processes that may play an important role in the evolution of faults, such as fluid flow, viscous deformation, dynamic stress changes, and subcritical crack growth, among other mechanisms, all of which could have their own time dependence. The modeling of fault slip and seismicity, and even more the characterization of the fault rheology based on seismicity or geodesy data, is thus a difficult challenge, in terms of finding which mechanism may be causing an observed time dependence. In this paper, we have added to this difficulty by demonstrating additional time-dependent behavior in the primary candidate, the rate and state friction law.

References

Ampuero, J., and A. M. Rubin (2008), Earthquake nucleation on rate and state faults: Aging and slip laws, *J. Geophys. Res.*, *113*, B01302, doi:10.1029/2007JB005082.

Bayart, E., A. M. Rubin, and C. Marone (2006), Evolution of fault friction following large velocity jumps, *Eos Trans. AGU*, *87*(52), Fall Meet. Suppl., Abstract S31A-0180.

Beeler, N. M., and D. A. Lockner (2003), Why earthquakes correlate weakly with the solid Earth tides: Effects of periodic stress on the rate and probability of earthquake occurrence, *J. Geophys. Res.*, *108*(B8), 2391, doi:10.1029/2001JB001518.

Beeler, N. M., T. E. Tullis, and J. D. Weeks (1994), The roles of time and displacement in the evolution effect in rock friction, *Geophys. Res. Lett.*, *21*, 1987–1990, doi:10.1029/94GL01599.

Belardinelli, M. E. (1997), Increase of creep interevent intervals: A conceptual model, *Tectonophysics*, *77*, 99–107, doi:10.1016/S0040-1951(97)00080-2.

Bilham, R. (1989), Surface slip subsequent to the 24 November 1987 Superstition Hills, California, earthquake monitored by digital creepmeters, *Bull. Seismol. Soc. Am.*, *79*, 424–450.

Boatwright, J., and M. Cocco (1996), Frictional constraints on crustal faulting, *J. Geophys. Res.*, *101*, 13,895–13,909.

Bodin, P., R. Bilham, J. Behr, J. Gomberg, and K. W. Hudnut (1994), Slip triggered on southern California faults by the 1992 Joshua Tree, Landers, and Big Bear earthquakes, *Bull. Seismol. Soc. Am.*, *84*, 806–816.

Boettcher, M. S., and T. H. Jordan (2004), Earthquake scaling relations for mid-ocean ridge transform faults, *J. Geophys. Res.*, *109*, B12302, doi:10.1029/2004JB003110.

Bourouis, S., and P. Bernard (2007), Evidence for coupled seismic and aseismic fault slip during water injection in the geothermal site of Soultz (France), and implications for seismogenic transients, *Geophys. J. Int.*, *169*, 723–732, doi:10.1111/j.1365-246X.2006.03325.x.

Bürgmann, R., S. Ergintav, P. Segall, E. H. Hearn, S. McClusky, R. E. Reilinger, H. Woith, and J. Zschau (2002), Time-space variable afterslip on and deep below the Izmit earthquake rupture, *Bull. Seismol. Soc. Am.*, *92*, 126–137.

Chlieh, M., et al. (2007), Coseismic slip and afterslip of the great M_w 9.15 Sumatra-Andaman earthquake of 2004, *Bull. Seismol. Soc. Am.*, *97*, doi:10.1785/0120050631.

Cochran, E. S., J. E. Vidale, and S. Tanaka (2004), Earth tides can trigger shallow thrust fault earthquakes, *Science*, *306*, 1164–1166.

Deng, J., M. Gurnis, H. Kanamori, and E. Hauksson (1998), Viscoelastic flow in the lower crust after the 1992 Landers, California, earthquake, *Science*, *282*, 1689–1692, doi:10.1126/science.282.5394.1689.

Dieterich, J. H. (1979), Modeling of rock friction: 1. Experimental results and constitutive equations, *J. Geophys. Res.*, *84*, 2161–2168.

Dieterich, J. H. (1992), Earthquake nucleation on faults with rate- and state-dependent strength, *Tectonophysics*, *211*, 115–134.

Dieterich, J. H. (1994), A constitutive law for the rate of earthquake production and its application to earthquake clustering, *J. Geophys. Res.*, *99*, 2601–2618.

Dieterich, J. H., V. Cayol, and P. Okubo (2000), The use of earthquake rate as a stress meter at Kilauea volcano, *Nature*, *408*, 457–460.

Di Toro, G., D. L. Goldsby, and T. E. Tullis (2004), Friction falls towards zero in quartz rock as slip velocity approaches seismic rates, *Nature*, *427*, 399–436, doi:10.1038/nature02249.

Dragert, H., K. Wang, and T. S. James (2001), A silent slip event on the deeper Cascadia subduction interface, *Science*, *292*, 1525–1528.

Du, W.-X., L. R. Sykes, B. E. Shaw, and C. H. Scholz (2003), Triggered aseismic fault slip from nearby earthquakes, static or dynamic effect?, *J. Geophys. Res.*, *108*(B2), 2131, doi:10.1029/2002JB002008.

Freed, A. M., R. Bürgmann, E. Calais, J. Freymueller, and S. Hreinsdóttir (2006a), Implications of deformation following the 2002 Denali, Alaska, earthquake for postseismic relaxation processes and lithospheric rheology, *J. Geophys. Res.*, *111*, B01401, doi:10.1029/2005JB003894.

Freed, A. M., R. Bürgmann, E. Calais, and J. Freymueller (2006b), Stress-dependent power-law flow in the upper mantle following the 2002 Denali, Alaska, earthquake, *Earth Planet. Sci. Lett.*, *252*, 481–489.

Goldsby, D. L., and T. E. Tullis (2002), Low frictional strength of quartz rocks at subseismic slip rates, *Geophys. Res. Lett.*, *29*(17), 1844, doi:10.1029/2002GL015240.

Gomberg, J., N. M. Beeler, M. L. Blanpied, and P. Bodin (1998), Earthquake triggering by transient and static deformation, *J. Geophys. Res.*, *103*, 24,411–24,426.

Gu, J.-C., J. R. Rice, A. L. Ruina, and S. T. Tse (1984), Slip motion and stability of a single degree of freedom elastic system with rate and state dependent friction, *J. Mech. Phys. Solids*, *32*, 167–196.

Guatteri, M., and P. Spudich (2000), What can strong-motion data tell us about slip-weakening fault-friction laws, *Bull. Seismol. Soc. Am.*, *90*, 98–116.

Hearn, E. H. (2003), What can GPS data tell us about the dynamics of post-seismic deformation?, *Geophys. J. Int.*, *155*, 753–777.

Hearn, E. H., R. Burgmann, and R. E. Reilinger (2002), Dynamic of Izmit earthquake postseismic deformation and loading of the Duzce earthquake hypocenter, *Bull. Seismol. Soc. Am.*, *92*, 172–193.

Heki, K., S. Miyazaki, and H. Tsuji (1997), Silent fault slip following an interplate thrust earthquake at the Japan Trench, *Nature*, *386*, 595–598.

Helmstetter, A., and B. E. Shaw (2006), Estimating stress heterogeneity from aftershock rate, *J. Geophys. Res.*, *111*, B07304, doi:10.1029/2005JB004077.

Helmstetter, A., G. Ouillon, and D. Sornette (2003), Are aftershocks of large Californian earthquakes diffusing?, *J. Geophys. Res.*, *108*(B10), 2483, doi:10.1029/2003JB002503.

Helmstetter, A., D. Sornette, J.-R. Grasso, J. V. Andersen, S. Gluzman, and V. Pisarenko (2004), Slider-block friction model for landslides: Implication for prediction of mountain collapse, *J. Geophys. Res.*, *109*, B02409, doi:10.1029/2002JB002160.

Helmstetter, A., Y. Kagan, and D. Jackson (2005), Importance of small earthquakes for stress transfers and earthquake triggering, *J. Geophys. Res.*, *110*, B05S08, doi:10.1029/2004JB003286.

Hirose, H., and K. Hirahara (2004), A 3-D quasi-static model for a variety of slip behaviors on a subduction fault, *Pure Appl. Geophys.*, *161*, 2417–2431, doi:10.1007/s00024-004-2573-7.

Hirose, T., and T. Shimamoto (2005), Slip-weakening distance of faults during frictional melting as inferred from experimental and natural pseudotachylytes, *Bull. Seismol. Soc. Am.*, *95*, 1666–1673.

Hsu, Y.-J., M. Simons, J.-P. Avouac, J. Galetzka, K. Sieh, M. Chlieh, D. Natawidjaja, L. Prawirodirdjo, and Y. Bock (2006), Frictional afterslip following the 2005 Nias-Simeulue earthquake, Sumatra, *Science*, *312*, 1921–1926, doi:10.1126/science.1126960.

Hsu, Y.-J., P. Segall, S.-B. Yu, L.-C. Kuo, and C. A. Williams (2007), Temporal and spatial variations of post-seismic deformation following the 1999 Chi-Chi, Taiwan earthquake, *Geophys. J. Int.*, *169*, 367–379.

Ide, S., and M. Takeo (1997), Determination of constitutive relations of fault slip based on seismic wave analysis, *J. Geophys. Res.*, *102*, 27,379–27,391.

Johnson, K. M., R. Bürgmann, and K. Larson (2006), Frictional properties on the San Andreas fault near Parkfield, California, inferred from models of afterslip following the 2004 earthquake, *Bull. Seismol. Soc. Am.*, *96*, S321–S338.

Kagan, Y. Y. (2004), Short-term properties of earthquake catalogs and models of earthquake source, *Bull. Seismol. Soc. Am.*, *94*, 1207–1228.

Langbein, J., J. R. Murray, and H. A. Snyder (2006), Coseismic and initial postseismic deformation from the 2004 Parkfield, California, earthquake, observed by global positioning system, electronic distance meter, creepmeters, and borehole strainmeters, *Bull. Seismol. Soc. Am.*, *96*, S304–S320.

Liu, Y., and J. R. Rice (2005), Aseismic slip transients emerge spontaneously in three-dimensional rate and state modeling of subduction earthquake sequences, *J. Geophys. Res.*, *110*, B08307, doi:10.1029/2004JB003424.

Liu, Y., and J. R. Rice (2007), Spontaneous and triggered aseismic deformation transients in a subduction fault model, *J. Geophys. Res.*, *112*, B09404, doi:10.1029/2007JB004930.

Lohman, R. B., and J. J. McGuire (2007), Earthquake swarms driven by aseismic creep in the Salton Trough, California, *J. Geophys. Res.*, *112*, B04405, doi:10.1029/2006JB004596.

Lowry, R. (2006), Resonant slow fault slip in subduction zones forced by climatic load stress, *Nature*, *442*, doi:10.1038/nature05055.

Marone, C. (1998), Laboratory-derived friction laws and their application to seismic faulting, *Ann. Rev. Earth Planet. Sci.*, *26*, 643–696.

Marone, C. J., C. H. Scholz, and R. Bilham (1991), On the mechanics of earthquake afterslip, *J. Geophys. Res.*, *96*, 8441–8452.

Marsan, D. (2006), Can coseismic stress variability suppress seismicity shadows? Insights from a rate-and-state friction model, *J. Geophys. Res.*, *111*, B06305, doi:10.1029/2005JB004060.

Melbourne, T., F. Webb, J. Stock, and C. Reigber (2002), Rapid postseismic transients in subduction zones from continuous GPS, *J. Geophys. Res.*, *107*(B10), 2241, doi:10.1029/2001JB000555.

Mitsui, N., and K. Hirahara (2006), Slow slip events controlled by the slab dip and its lateral change along a trench, *Earth Planet. Sci. Lett.*, *245*, 344–358.

Miyazaki, S., P. Segall, J. Fukuda, and T. Kato (2004), Space time distribution of afterslip following the 2003 Tokachi-oki earthquake: Implications for variations in fault zone frictional properties, *Geophys. Res. Lett.*, *31*, L06623, doi:10.1029/2003GL019410.

Montési, L. G. J. (2004), Controls of shear zone rheology and tectonic loading on postseismic creep, *J. Geophys. Res.*, *109*, B10404, doi:10.1029/2003JB002925.

Nur, A., and J. R. Booker (1972), Aftershocks caused by pore fluid flow?, *Science*, *175*, 885–887.

Nur, A., and G. Mavko (1974), Postseismic viscoelastic rebound, *Science*, *18*, 204–206, doi:10.1126/science.183.4121.204.

Peng, Z., J. E. Vidale, M. Ishii, and A. Helmstetter (2007), Anomalous seismicity rate immediately before and after mainshock rupture from high-frequency waveforms in Japan, *J. Geophys. Res.*, *112*, B03306, doi:10.1029/2006JB004386.

Perfettini, H., and J.-P. Ampuero (2008), Dynamics of a velocity strengthening fault region: Implications for slow earthquakes and postseismic slip, *J. Geophys. Res.*, *113*, B09411, doi:10.1029/2007JB005398.

Perfettini, H., and J.-P. Avouac (2004), Postseismic relaxation driven by brittle creep: A possible mechanism to reconcile geodetic measurements and the decay rate of aftershocks, application to the Chi-Chi earthquake, Taiwan, *J. Geophys. Res.*, *109*, B02304, doi:10.1029/2003JB002488.

Perfettini, H., and J.-P. Avouac (2007), Modeling afterslip and aftershocks following the 1992 Landers earthquake, *J. Geophys. Res.*, *112*, B07409, doi:10.1029/2006JB004399.

Perfettini, H., J.-P. Avouac, and J.-C. Ruegg (2005), Geodetic displacements and aftershocks following the 2001 M_w = 8.4 Peru earthquake: Implications for the mechanics of the earthquake cycle along subduction zones, *J. Geophys. Res.*, *110*, B09404, doi:10.1029/2004JB003522.

Pollitz, F. F., M. Nyst, T. Nishimura, and W. Thatcher (2006), Inference of postseismic deformation mechanisms of the 1923 Kanto earthquake, *J. Geophys. Res.*, *111*, B05408, doi:10.1029/2005JB003901.

Pritchard, M. E., and M. Simons (2006), An aseismic slip pulse in northern Chile and along-strike variations in seismogenic behavior, *J. Geophys. Res.*, *111*, B08405, doi:10.1029/2006JB004258.

Ranjith, K., and J. R. Rice (1999), Stability of quasi-static slip in a single degree of freedom elastic system with rate and state dependent friction, *J. Mech. Phys. Solids*, *47*, 1207–1218.

Reasenberg, P. A., and L. M. Jones (1994), Earthquake aftershocks: Update, *Science*, *265*, 1251–1252.

Reinen, L. A. (2000), Slip styles in a spring-slider model with a laboratory-derived constitutive law for serpentinite, *Geophys. Res. Lett.*, *27*, 2037–2040.

Rice, J. R., and J.-C. Gu (1983), Earthquake aftereffects and triggered seismic phenomena, *Pure Appl. Geophys.*, *121*, 187–219.

Rubin, A. M., and J.-P. Ampuero (2005), Earthquake nucleation on (aging) rate and state faults, *J. Geophys. Res.*, *110*, B11312, doi:10.1029/2005JB003686.

Ruina, A. (1983), Slip instability and state variable friction laws, *J. Geophys. Res.*, *88*, 10,359–10,370.

Savage, J. C., J. L. Svarc, and S.-B. Yu (2007), Postseismic relaxation and aftershocks, *J. Geophys. Res.*, *112*, B06406, doi:10.1029/2006JB004584.

Schaff, D. P., G. C. Beroza, and B. E. Shaw (1998), Postseismic response of repeating aftershocks, *Geophys. Res. Lett.*, *25*, 4549–4552.

Scholz, C. H. (1990), *The Mechanics of Earthquake and Faulting*, Cambridge Univ. Press, New York.

Scholz, C. H., M. Wyss, and S. W. Smith (1969), Seismic and aseismic slip on the San Andreas fault, *J. Geophys. Res.*, *74*, 2049–2069.

Segall, P., E. Desmarais, D. Shelly, A. Miklius, and P. Cervelli (2006), Earthquakes triggered by silent slip events on Kilauea volcano, Hawaii, *Nature*, *442*, 71–74.

Shibazaki, B., and Y. Iio (2003), On the physical mechanism of silent slip events along the deeper part of the seismogenic zone, *Geophys. Res. Lett.*, *30*(9), 1489, doi:10.1029/2003GL017047.

Szeliga, W., T. Melbourne, M. Santillan, and M. Miller (2008), GPS constraints on 34 slow slip events within the Cascadia subduction zone, 1997–2005, *J. Geophys. Res.*, *113*, B04404, doi:10.1029/2007JB004948.

Takai, K., H. Kumagai, and N. Fujii (1999), Evidence for slow slip following a moderate-size earthquake (Mw = 5.7) in a subducting plate, *Geophys. Res. Lett.*, *26*, 2113–2116, doi:10.1029/1999GL900465.

Tsutsumi, A., and T. Shimamoto (1997), High-velocity frictional properties of gabbro, *Geophys. Res. Lett.*, *24*, 699–702.

Wennerberg, L., and R. V. Sharp (1997), Bulk friction modeling of afterslip and the modified Omori law, *Tectonophysics*, *277*, 109–136.

Wesson, R. L. (1988), Dynamics of fault creep, *J. Geophys. Res.*, *93*, 8929–8951, doi:10.1029/88JB00134.

Yoshida, S., and N. Kato (2003), Episodic aseismic slip in a two-degree-of-freedom block-spring model, *Geophys. Res. Lett.*, *30*(13), 1681, doi:10.1029/2003GL017439.

_____

A. Helmstetter, Laboratoire de Géophysique Interne et Tectonophysique, Université Joseph Fourier and Centre National de la Recherche Scientifique, Grenoble, France. (ahelmste@obs.ujf-grenoble.fr)

B. Shaw, Lamont-Doherty Earth Observatory, Columbia University, 61 Route 9W, Palisades, NY 10964, USA. (shaw@ldeo.columbia.edu)